The effects of air and underwater blast on composite sandwich panels and tubular laminate structures

H. Arora, P. Hooper and J. P. Dear

Department of Mechanical Engineering, Imperial College London, SW7 2AZ

Corresponding Author: Dr John P. Dear
Email: j.dear@imperial.ac.uk
Tel: +44 207 594 7086

Keywords: Air blast, underwater blast, shock, sandwich structures, composites

Abstract

The resistance of glass-fibre reinforced polymer (GFRP) sandwich panels and laminate tubes to blast in air and underwater environments has been studied. Procedures for monitoring the structural response of such materials during blast events have been devised. High-speed photography was employed during the air-blast loading of GFRP sandwich panels, in conjunction with digital image correlation (DIC), to monitor the deformation of these structures under shock loading. Failure mechanisms have been revealed by using DIC and confirmed in post-test sectioning. Strain gauges were used to monitor the structural response of similar sandwich materials and GFRP tubular laminates during underwater shocks. The effect of the backing medium (air or water) of the target facing the shock has been identified during these studies. Mechanisms of failure have been established such as core crushing, skin/core cracking, delamination and fibre breakage. Strain gauge data supported the mechanisms for such damage. These studies were part of a research programme sponsored by the Office of Naval Research (ONR) investigating blast loading of composite naval structures. The full-scale experimental results presented here will aid and assist in the development of analytical and computational models. Furthermore, it highlights the importance of support and boundary conditions with regards to blast resistant design.

1 Introduction

The study reported here forms part of a programme to investigate the retention of integrity of composite structures subject to increasingly demanding conditions. When designing against such threats one has to consider the blast event (pressure wave), the surroundings (fluid medium and boundary conditions) and the component (material properties and construction). The research presented here focuses on air-blast loading of glass-fibre reinforced polymer (GFRP) sandwich composite panels and underwater-blast loading of GFRP sandwich composite panels and tubular laminates.

Several studies have investigated the dynamic deformations due to explosive blast loading on plates. Neuberger et al. [1, 2] highlighted several early studies, which classified failure modes of structures under impulse loading, from large inelastic deformation to tearing and shear failure at the supports. Rather than using explosives to generate shocks, shock tubes have been shown to be a favourable alternative used extensively in shock/blast simulation studies. Tekalur et al. [3-5] have experimentally studied the effect of blast loading using shock tubes and controlled explosion tubes loading on E-glass fibre based composites and other materials. Results suggested that the E-glass fibre composite experienced progressive damage during high-rate loading of the same nature as described by Hoo Fatt and Palla [6], with progressive front face failure due to indentation followed by complete core collapse. These studies have been continually developed by the same research group to great effect, with many parameters being examined such as the distribution of blast energy during the impact process [7] and retention of integrity of sandwich structures due to blast loads [8].

Changing the medium used to carry the shock from a gas to a liquid (increasing the density) increases speed of sound and generates a significant rise in pressures produced by a blast event. It is for these and related reasons that underwater shocks and their interaction with surrounding submerged structures are of particular interest to the naval industry. When an explosion occurs underwater, there is an intense release of energy, high pressure and heat, similar to the air blast case. This is relieved by the formation of an intense (compressive) pressure wave, or shock wave, which radiates away from the source. However with an underwater explosion, there is also the formation of high-pressure gas bubble, which is formed by the expanding reaction products formed during the explosion. The pressure within this bubble is significantly higher than hydrostatic and therefore the bubble radius increases rapidly. However, due to inertial and other effects, the gas bubble expands too far until the hydrostatic pressure is greater than the pressure within the gas bubble. The bubble then contracts once more until it contracts too far. There are a series of overshoots and undershoots during this process until all the energy is dissipated in one way or another. The movement and dynamic behaviour of the bubble is influenced by a number of factors including the proximity to the air-water interface, other surfaces and turbulence [9]. In terms of energy released, approximately 47% goes towards the formation and pulsation of the bubble and the remainder to the shock wave [10]. If stand-off distance can be assumed to be large, then the effect of the bubble can be ignored, and this seems to be the focus of most authors, highlighted by Panciroli and Abrate [11].

Considerable care is needed to instrument underwater explosive experiments to obtain the required data. Therefore, different laboratory experimental techniques are employed by researchers. For example, the principle of a shock tube has been applied to water blast simulations using the water-hammer effect. Deshpande et al. [12] investigated the fluid structure interaction (FSI) of sandwich plates with steel face sheets and aluminium foam cores. A strong FSI effect was observed experimentally and a coupled finite element (FE) analysis was able to capture the measured degree of core compression unlike the decoupled analysis, which underestimated the degree of core compression. This illustrated the importance of FSI and having a coupled analysis during such events. This water hammer technique has been used elsewhere incorporating moiré shadow interferometry techniques to obtain full field out-of-plane deformation profiles by Espinosa et al. [13]. This method was also employed by LeBlanc and Shukla [14] with in-depth finite element (FE) analyses forming agreements in terms of damage generated in the composite laminates studied.

This investigation highlights the mechanisms of failure observed within commercially available naval materials and improves the understanding behind the sequence of events responsible for such damage. This is with the aim of improving computational simulations and hence the design process for marine structures.

2 Materials

Two types of targets were evaluated, shown schematically in Figure 1. Sandwich panels were constructed using 2 plies of (0°/90°/±45°) E-glass quadriaxial skins with (manufacturer code QE1200) on an SAN foam core (manufacturer code P800) infused with a Prime-LV epoxy resin. Various core thicknesses were tested from 15 to 40 mm. The exposed target areas for the air-blast and underwater-blast experiments were 1.6 m x 1.3 m and 0.4 m x 0.3 m respectively. The two different sized panels were designed to have a comparable aspect ratio. The larger panels, used for the air-blast, were to represent full-scale face-panels of comparable magnitude to real naval structures. Smaller samples were required for the underwater blast experiments to allow for sufficient rigid edge restraint/support during tests as well as manoeuvrability of the entire rig during test set-up. The smaller targets kept within sensible bounds of the test facility in terms of the size of test pond, explosives used, desired maximum pressures and hence blast parameters (suitable guidelines for such underwater test designs are outlined in [15]). The size of the panels (length to thickness ratio) was also chosen to keep the behaviour of the structure to that of a plate i.e. allow for typical bending response to occur. Sandwich materials were provided by SP Gurit manufactured by P.E. Composites.

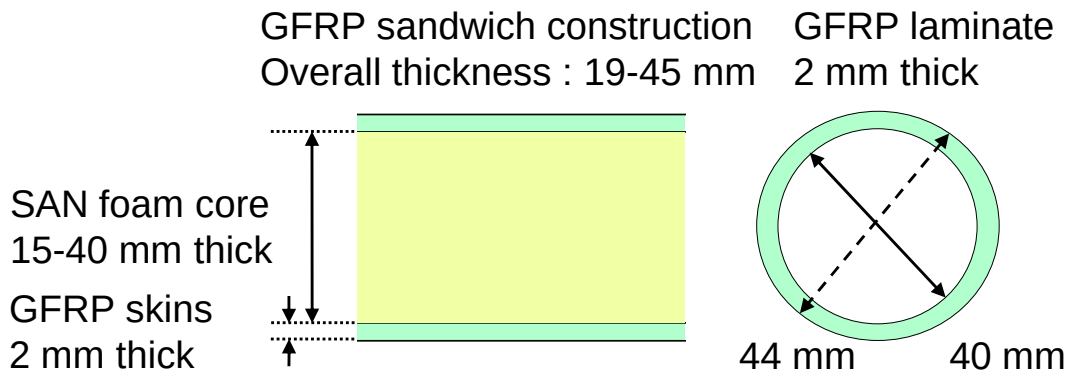

Figure 1: Target constructions: sandwich panels (left) and tubular laminate (right).

The composite tube construction was 40 mm inner diameter, 44 mm outer diameter made from 8H Satin weave 300g/m^2 (excluding CYCOM® 919 epoxy resin impregnation) known as weave style US 7781. The tube was constructed from 9 plies of 7781 epoxy rubber toughened thermoset E-glass fabric. The fabric weave style was selected as the mechanical properties are similar in both the warp and weft directions, simplifying the construction process. The exposed target length was 0.3 m. This size of target was chosen to allow for both the cross-sectional/circumferential and axial (bending) deformation to be observed. Tubular laminates were sourced from Tri-Cast. Table 1 shows a summary of the material properties provided by the manufacturer.

Table 1: Summary of materials used in the GFRP sandwich panels and tubular laminates.

Material	QE1200	P800	CYCOM 919-7781
Density (kg/m^3)	1750	155	1320
Tensile modulus (GPa)	17	0.14	3.9
Compressive modulus (GPa)	-	0.13	4.2
Tensile strength (MPa)	260	-	68
Compressive strength (MPa)	200	2.8	70
Shear modulus (MPa)	6500	61	-
Tensile failure strain (%)	≥1.5	-	≥1.7

3 Experimental

3.1 Air blast loading of GFRP sandwich panels

GFRP sandwich panels were subject to full-scale air-blast loading to observe the deformation and damage development within such typical marine constructions. An overview of the test configurations is shown in Figure 2 (see Figure 2(a) for air blast studies). Full-field displacement plots of the back face of the target were obtained for the duration of the blast event by employing high-speed photography in conjunction with digital image correlation (DIC) methods. Two high-speed video cameras (Photron SA3s) were positioned behind the 1.6 m x 1.3 m speckled targets and sampled at 2000 frames/second at full resolution (1024 x 1024 pixels). This sampling frequency, required to suitably capture the event, was decided using a single degree of freedom model based on the procedure outlined by Biggs [16]. The time taken to reach maximum deflection for an example blast (1.5 bar peak shock pressure) was established for each target to be within the region of 5 ms. Therefore by using the Photron SA3 cameras it was possible to operate at full resolution (keeping spatial resolution high), whilst capturing the images at a suitable rate (temporal resolution) for the DIC analysis to be conducted. These cameras were calibrated prior to testing to allow the recorded images to be processed in ARAMIS (produced by GOM mbH), the DIC software used to perform the image correlation calculations. A laser gauge was positioned on a steel beam mount as a secondary point measurement tool focussing on the centre of the panel, which sampled at 2000 Hz. The purpose of the laser gauge was to verify the results taken from the high-speed video recordings. Instrumentation is shown in Figure 3 with the DIC set-up and laser gauge arrangement featured in Figure 3(a).

3.2 Air blast test design and other instrumentation

Reflected pressure and static (side-on) pressure measurements were taken at the same stand-off distance from the charge as the target. High-speed video cameras were also positioned externally on the test pad, shielded in turrets, to capture front-face deformation as shown in Figure 2(a). Three targets were tested; two with a 40 mm thick core (denoted G1) and one with a 30 mm core (denoted G2). The blast parameters used during the tests shown here were 30 kg C4 charge at a stand-off distance of 8 m and 14 m. The tests conducted at a 14 m stand-off distance (an equivalent peak shock pressure of approximately 2 bar) were designed to take the panels to their elastic limit. FE simulations were conducted in ABAQUS to design the panel geometries, predicting the central peak deflections and peak

surface strains below failure magnitudes (stated in Table 1). The blast of 30 kg C4 at 8 m stand-off was designed to inflict damage on the target.

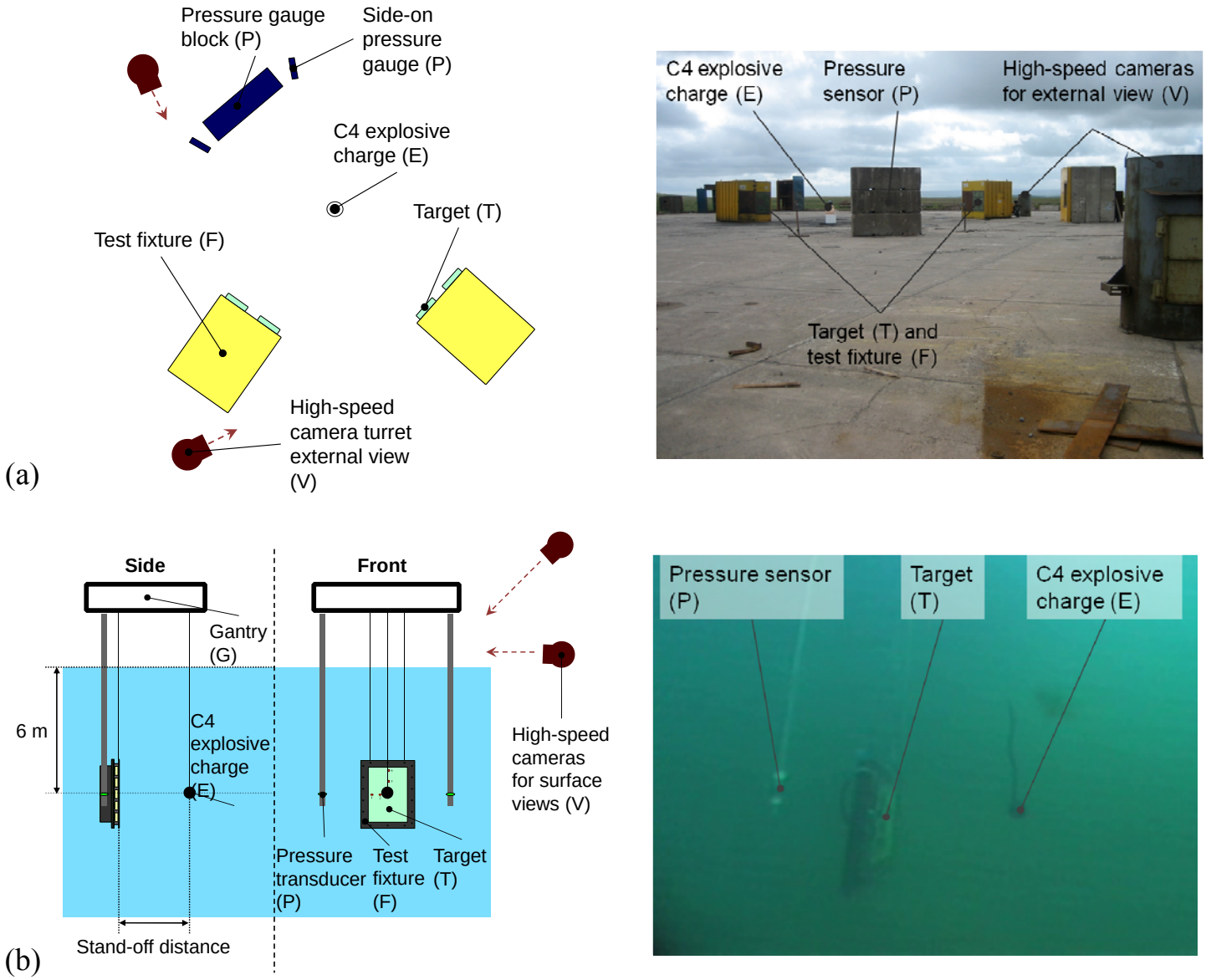

Figure 2: Blast configurations showing schematic diagrams and images of the test set-up: (a) Air blast and (b) Water blast. Featured in each diagram are: targets to be tested (T), sample fixtures (F), high-speed cameras and their relative locations (V), pressure sensor arrangements (P), gantry for the underwater tests (G) and C4 explosive charge (E).

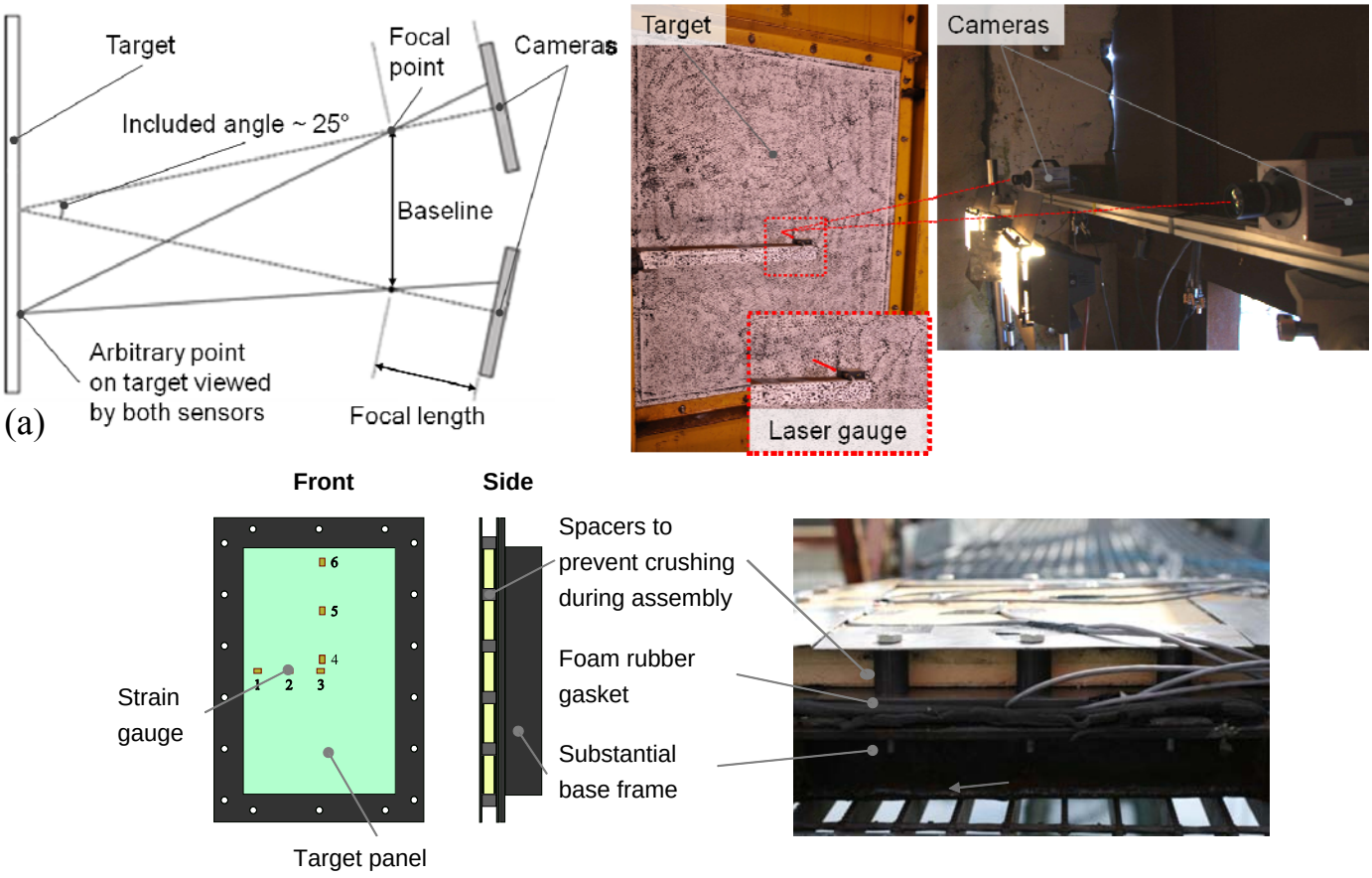

Figure 3: Instrumentation: (a) Air blast featuring the DIC set-up and position of laser gauge; (b) Strain gauge arrangement for underwater blast loading of sandwich panels; (c) composite tubes.

3.3 Underwater blast loading of GFRP sandwich panels

GFRP sandwich panels were subject to underwater-blast loading to observe the deformation of the targets during the blast and damage sustained. A comparison can be made between the air and

underwater blast cases as to differences in behaviour. Surface strain measurements were taken during the blast event using strain gauges positioned at 12 different locations. They were positioned along centre-lines of the panel face: three on the horizontal spaced evenly at 60 mm intervals from the centre and three on the vertical spaced evenly at 80 mm intervals 10 mm from the centre to avoid overlap of gauges. The other six gauges were positioned behind these locations on the rear face (shown in Figure 3(b)). The strain gauges (and data acquisition hardware) chosen for this application was chosen specifically with the ability to monitor dynamic events (in terms of strain magnitude and strain rate). Once the gauges were bonded they were sealed in accordance to recommendations from engineers at Vishay Micro-Measurements to insulate from the environment and protect during impact, whilst maintaining a low profile and mass [17].

The panels were first bonded into a steel frame (3 mm thick mild steel). They were then bolted into a substantial base frame, comprising 10 mm thick mild steel, prior to testing. The base frame was designed to mitigate the effects of the blast wave wrapping around the target and interfering with its response to the incident wave acting on the front face. It also provided an enclosed volume behind the back-face of the panel to hold either air or water, which represents the conditions existing in a significant portion of a naval vessel. Thirdly it provided a weighty structure on its edges to replicate the boundary conditions experienced by a similar panel on the hull of a ship (from the support framework). A rubber foam gasket was used to create a seal for the backing fluid and to minimise the damage caused to the cables connected to the strain gauges on the rear face. Steel tube spacers were used to avoid crushing of the core material of the test panels, when bolted into the heavy base frame. These features are shown in Figure 3(b).

3.4 Underwater blast loading of GFRP tubular laminates

GFRP tubes were subject to underwater blast loads to assess how a tubular structure, a curved geometry, responds to such loads. Eight tubes were tested, seven filled and sealed with air inside (AF) and one with water (WF). One set of AF and WF tubes were paired to investigate the effect of the filling medium on the response of the tubes. The remainder of the air-filled tubes were tested in pairs and subjected to progressively increasing shock pressures to observe the damage inflicted on such constructions over a range of shock pressures. The sites thought to experience high principal stress during loading are at the ends of each tube on the front face (aligned square-on to the shock) and in the centre on the back face (this was also observed by [18] during similar aluminium shell trials). The two main motions observed during an underwater blast, bending and, what is commonly termed, breathing. These were deemed to be best observed by positioning three gauges axially, one at either end on the front and one at the centre on the back face, and three gauges circumferentially at the centre of the tube at 90° intervals (shown in Figure 3(c)). The tubes were bonded into aluminium end-tabs and then bolted into a heavy steel frame, restraining the tube ends in all six degrees of freedom. This arrangement is shown in Figure 3(c).

3.5 Underwater blast test design and other instrumentation

High-speed video cameras were positioned on the test pad to capture the surface waves and disturbances during the blast from several angles. Static (side-on) pressure measurements were taken either side of the target using Neptune Sonar shock gauges. These were mounted on steel scaffold poles and lowered to the mid-height of the target. Details of the set-up are shown in Figure 2(b). Two panel targets were tested, one a 30 mm thick core (denoted G3) with air as the supporting fluid on the rear face and the other a 15 mm thick core (denoted G4) with water the supporting fluid. Blast parameters for the panel tests were 1 kg C4 charge at 6 m depth and a stand-off distance of 1.0 m and 1.4 m respectively. These blasts were designed to cause significant damage to the targets to observe any trends regarding effects of backing fluid and differences between air-shock and underwater-shock regimes. The tubes were subject to a range of blast parameters, which involved using 0.5-1.0 kg C4 charges over a range of stand-off distances from 1.0 to 2.0 m at a 6 m depth. The details for specific tests will be mentioned alongside the results. The intention here was to also inflict significant damage to the tube structures, specifically, to observe progressive levels of damage in the air-filled tubes and highlight any effects of the filling medium on the observed response.

All positions of targets, charge and pressure sensors were verified using a submarine camera, prior to testing featured in Figure 2(b).

Results

3.6 Air blast of GFRP sandwich composite panels

The two targets were both initially subject to the same explosive charge (30 kg of C4) at the same stand-off distance (14 m). Figure 4 shows sample images taken from the high-speed videos positioned on the test pad. The shock wave is seen to arrive at the target 20 ms after detonation. This blast scenario was designed to take the panels to their elastic limit as stated in the Section 3.1.

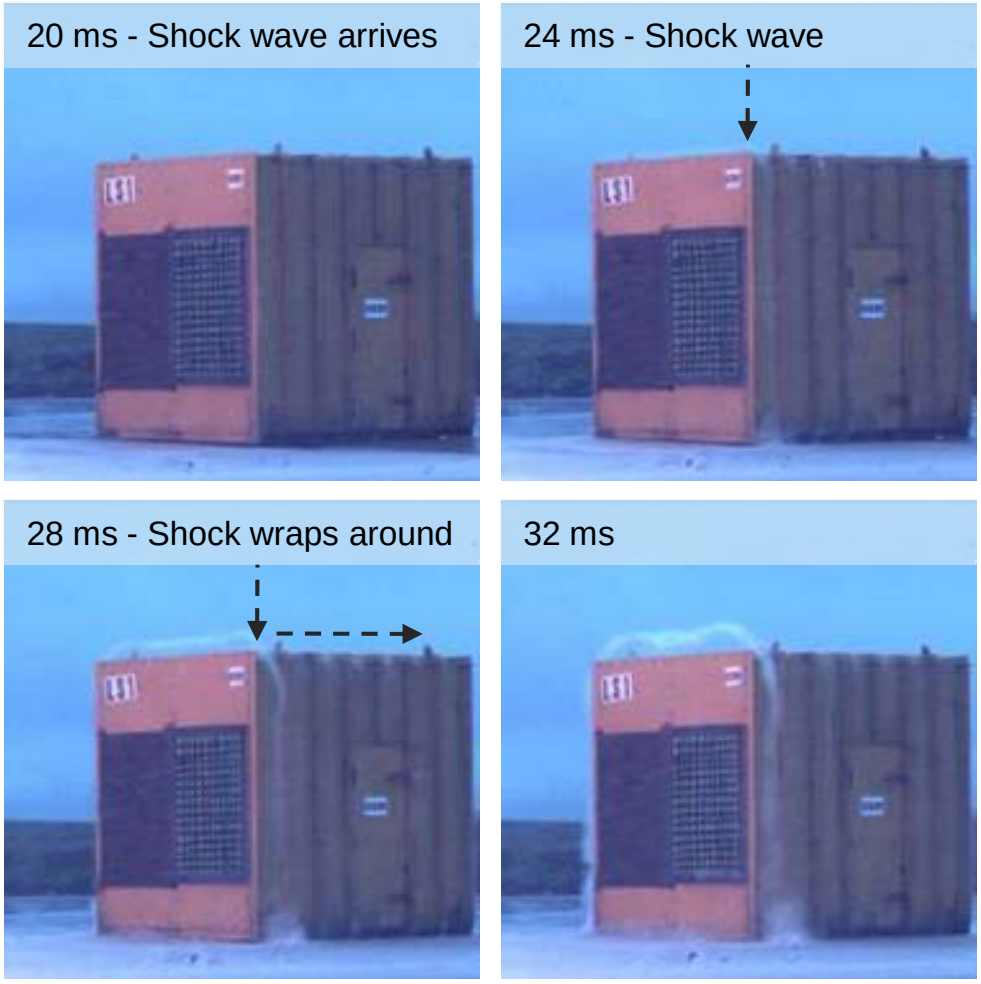

Figure 4: Images of the shock wave impinging on the test sample (at 20 ms) and wrapping around the test cubicle thereafter (sandwich panel G1 with core thickness 40 mm and charge of 30 kg charge at stand-off of 14 m).

Figures 5 and 6 give a direct comparison between the target sandwich panels, G1 (40 mm core) and target G2 (30 mm core), with regard to their response to a given air-blast load. It can be seen that increasing the core thickness lowers the amplitude of oscillations. This is due to the increased stiffness of the plate, resulting from the increased core thickness.

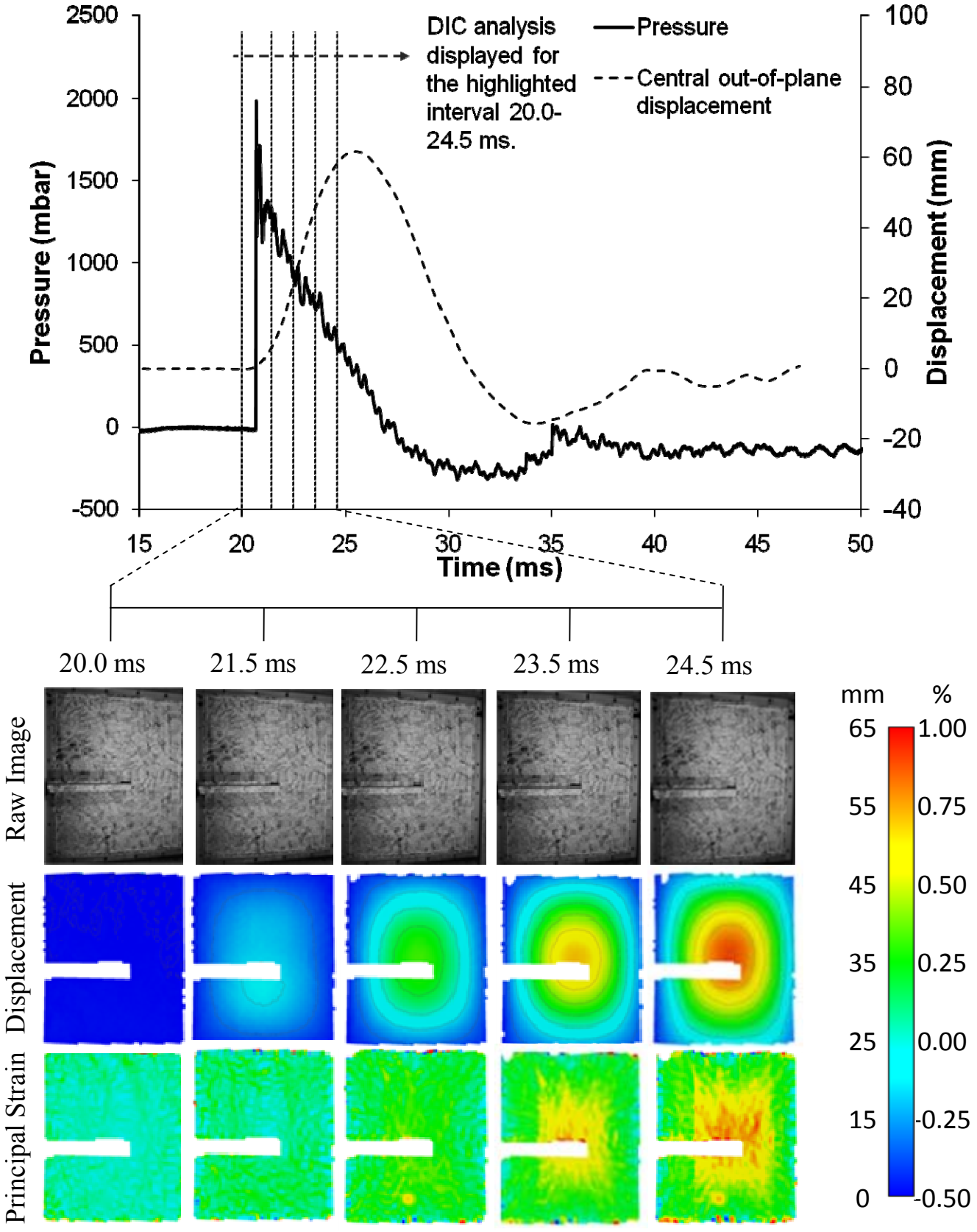

Figure 5: Transient reflected pressure recording and the central out-of-plane displacement of panel G1 (core thickness 40 mm) during blast loading (30 kg at 14 m stand-off) showing high-speed images of the back-face of the target with analysed results from ARAMIS. The white line from the left hand edge to the centre is the region of the specimen obscured by the laser gauge (visible in the raw images). Images are displayed from the point of shockwave arrival at the target 20 ms after detonation.

Figure 5 shows the central point deflection of G1 subjected to a recorded peak pressure of 2 bar (30 kg of C4 at stand-off of 14 m). Back-face images taken from the high-speed photography are also shown alongside the computed results from the image correlation in the form of contour plots of out-of-plane displacement and principal strain for the various times highlighted. Note that the white line from the left hand edge to the centre in the contour plots is the region of the specimen obscured by the laser gauge and its mount. G1 was seen to deflect to a maximum distance out-of-plane of 63 mm (whilst Figure 6 shows G2 deflected 78 mm). These deflection measurements agreed well with the laser gauge measurements for this single (central) point data, details to be discussed later in section 4.1. The level of major principal strain peaked in the region of 1% on the back face for G1. The G1 panel was deformed within a limit such that no visible damage was sustained. There were no obvious signs of damage shown within the DIC analysis for G1.

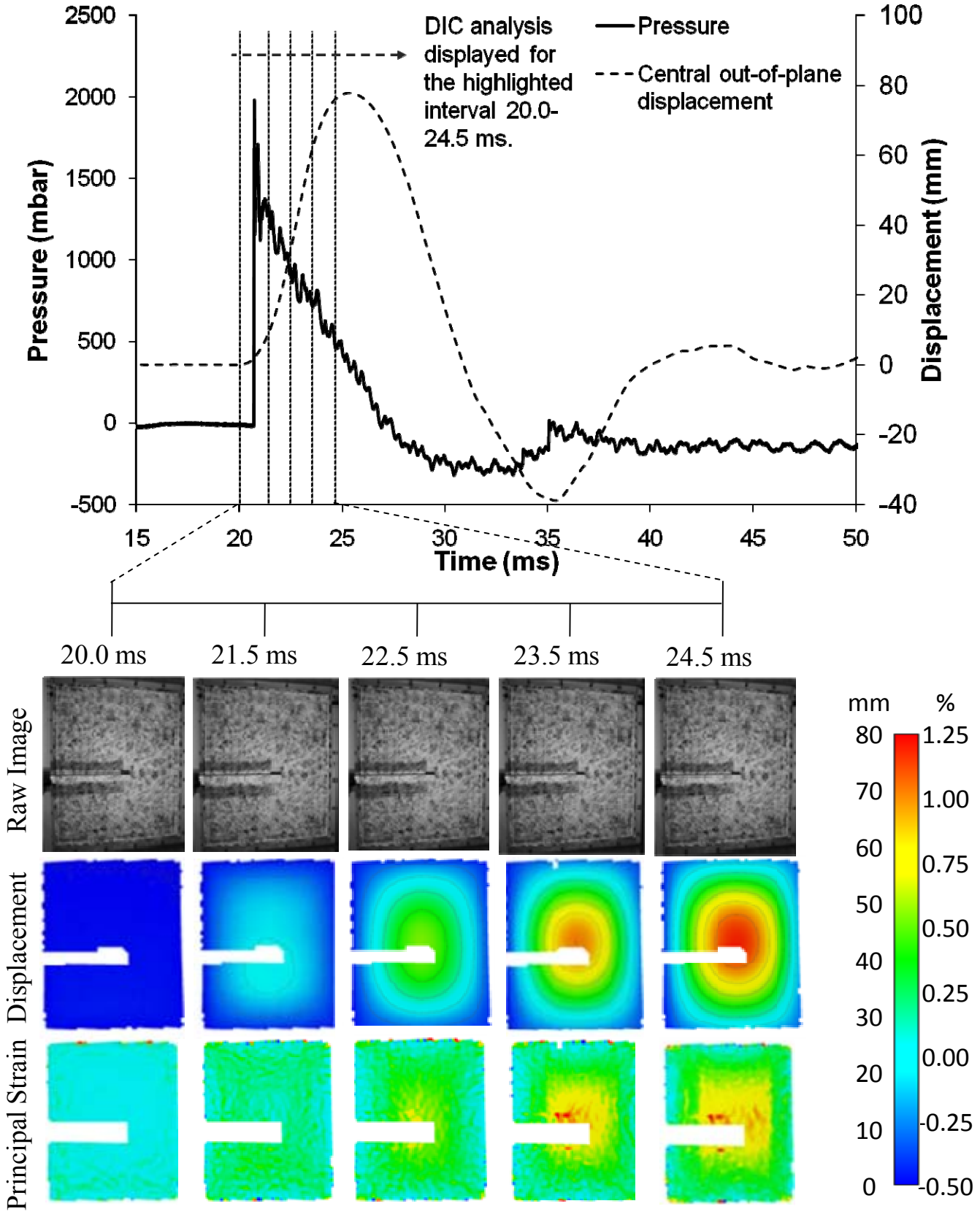

Figure 6: Transient reflected pressure recording and the central out-of-plane displacement of panel G2 (core thickness 30 mm) during blast loading (30 kg at 14 m stand-off) showing high-speed images of the back-face of the target with analysed results from ARAMIS. Images are displayed from the point of shockwave arrival at the target 20 ms after detonation.

A similar response was exhibited in Figure 6 for G2 with its reduced core thickness when subjected to a recorded peak pressure of 2 bar (30 kg of C4 at stand-off of 14 m). For G2, surface strains peaked at 1.25% and below the expected failure strains of the fibres. The lower limit (assuming a linear elastic relationship) for fibre strain to failure is 1.4% (as stated in Table 1). Signs were, however, observed within the DIC analysis that mild sub-surface core cracking had occurred. Early discontinuities in the major principal strain plots indicate possible detachment of the skin from the core i.e. possible cracking. This was confirmed upon sectioning of the panel after the blast.

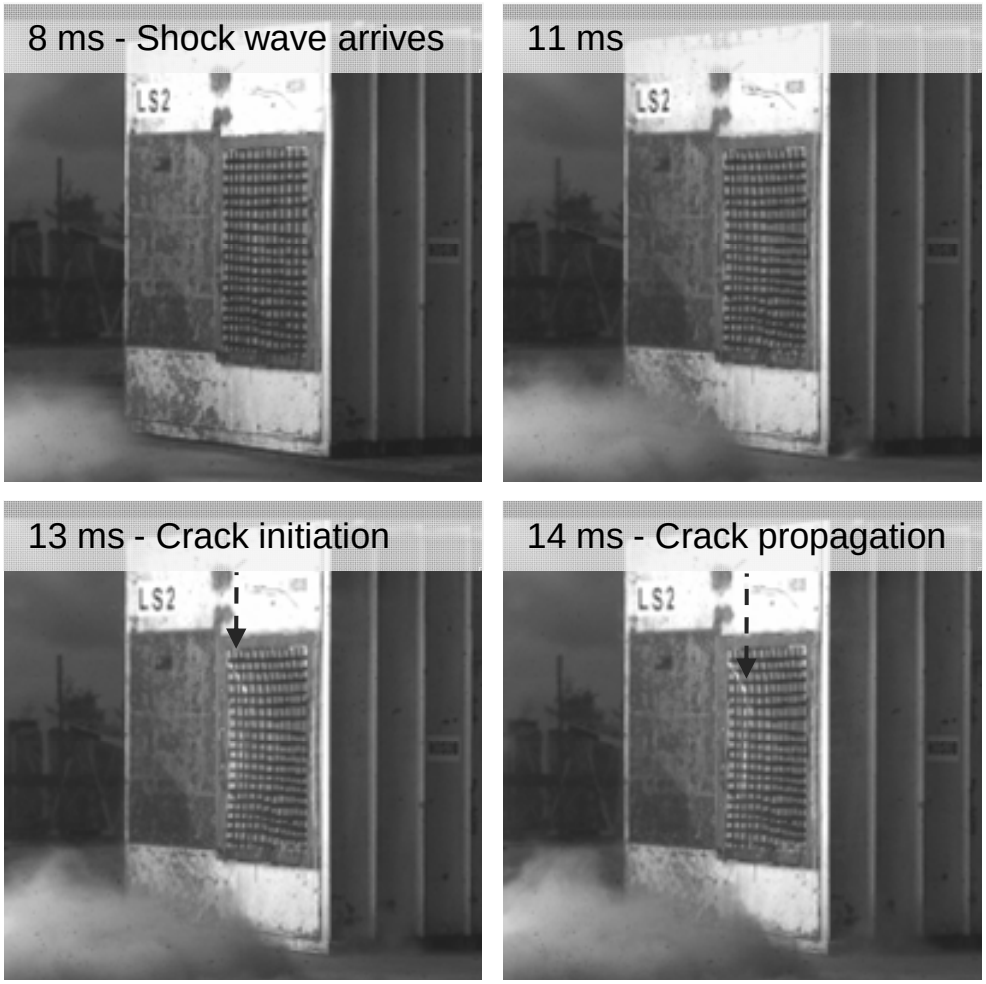

Figure 7: Images of the shock wave impinging on the test sample (8 ms) causing deformation and front-skin damage thereafter (sandwich panel G1 with core thickness 40 mm and charge of 30 kg charge at stand-off of 8 m).

As the DIC analysis agreed with predictions for peak elastic displacements of the targets due to a 2 bar shock pressure, and both the DIC analysis and visual inspection showed no visible skin damage to panel G1, it was decided that another panel of the same construction as G1 be subject to a more substantial blast to induce significant skin and core damage. This highlighted clearly the failure diagnostic capabilities of the DIC technique in this context. Blast parameters for this final air blast involved a 30 kg charge positioned at a reduced stand-off of 8 m from G1. Figure 7 shows the progressive deformation and eventual skin damage inflicted on G1 by the 8 bar pressure shock wave. A skin crack is seen to originate from the top left hand edge of the panel and propagate down that side of the target.

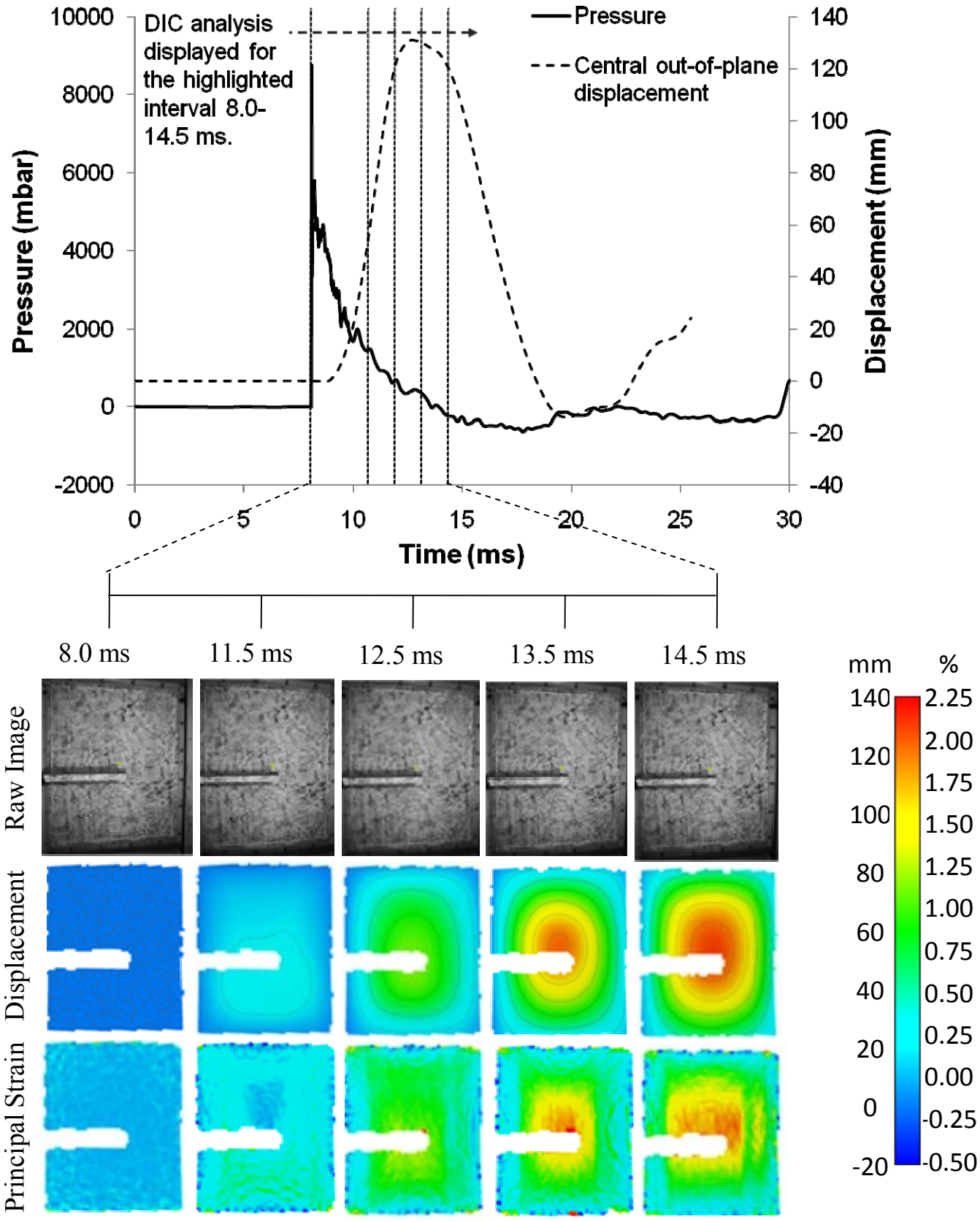

Figure 8: Transient reflected pressure recording and the central out-of-plane displacement of panel G1 (core thickness 40 mm) during blast loading (30 kg at 8 m stand-off) showing high-speed images of the back-face of the target with analysed results from ARAMIS. Images are displayed from the point of shockwave arrival at the target 8 ms after detonation.

Figure 8 shows the measured reflected pressure as well as the central out-of-plane displacement during the blast event for G1 with at 30 kg charge at stand-off of 8 m. Comparing this plot of out-of-plane displacement to that shown earlier in Figure 5, asides from the magnitude of peak out-of-plane displacement, immediately one can notice the difference in smoothness of the path taken during the first oscillation. Looking closely at the time period 12.5-13.5 ms, one can observe a flattening in the displacement curve near its maximum condition. This coincides with the time (13 ms) when the crack is observed to form in Figure 7.

The peak out-of-plane displacement was 131 mm and strains peaked in the region of 3% prior to the crack developing. Upon post inspection, the front face sustained inter-laminar skin failure and front-ply fibre breakage whilst the core suffered a severe skin-to-skin crack (see Figure 9). Towards the centre of the panel, the severity of the failure increased.

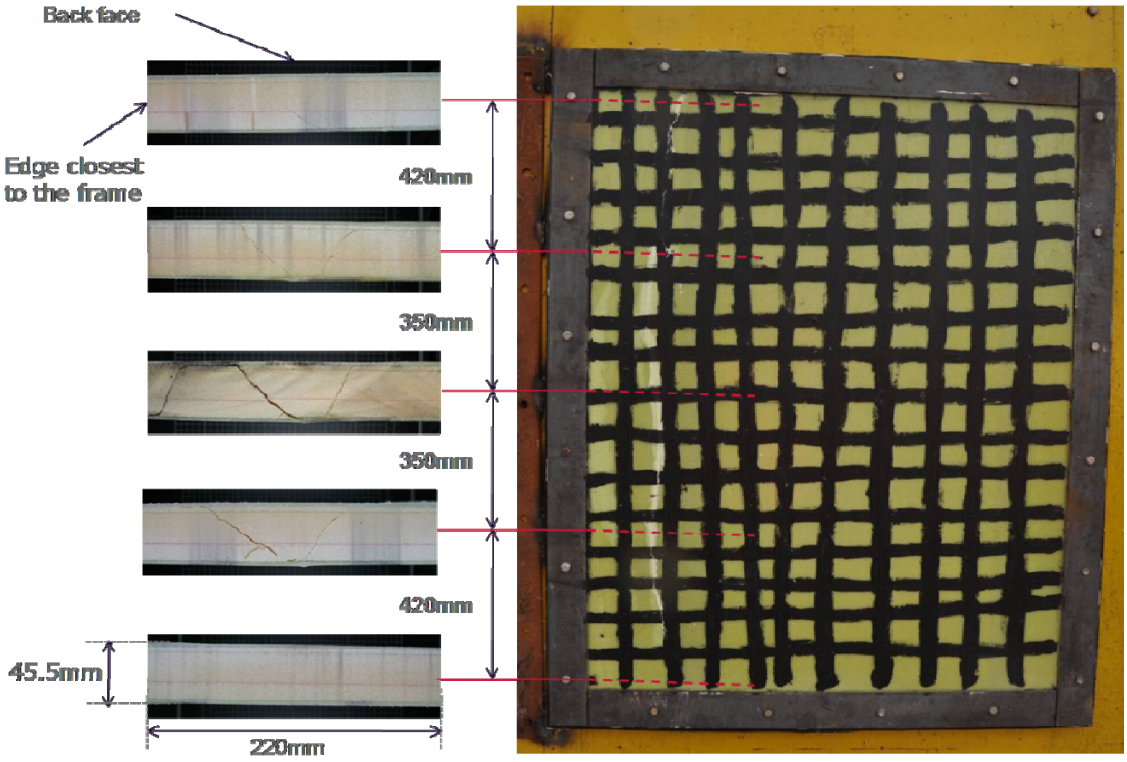

Figure 9: Front face damage: The whole panel with a clear crack down the left-hand edge of the panel (right), sectioned at regular intervals showing various failure mechanisms (left). This is for sandwich panel G1 with core thickness 40 mm and charge of 30 kg charge at stand-off of 8 m.

3.7 Underwater blast loading of GFRP sandwich panels

Two sandwich panel targets, G3 (30 mm core thickness) and G4 (15 mm core thickness), were subject to 2 different blast scenarios. There were two different impulses and two different sets of boundary conditions to explore the effect of the backing (or supporting) medium to the target's response. A 1 kg C4 explosive charge was set at the mid-height of the target 6 m below the surface of the water at a stand-off distance of 1 m for G3 with an air-pocket encapsulated behind the target. G4 had the 1 kg

charge of C4 1.4 m away at the same depth but this time with water encapsulated behind the target. Although only a 1 kg charge was used this was still substantial given the transition from air blasting to underwater.

Surface effects propagating from the blast event were recorded and sample images are shown in Figure 10. The sequence runs through the initial shock producing a spray at the surface at about 5 ms, which remains until the bubble begins to rise, forming a dome at the surface after the first 1000 ms. This reaches a peak height of approximately 1 m prior to venting at 1400 ms, throwing a large mass of water up in the air.

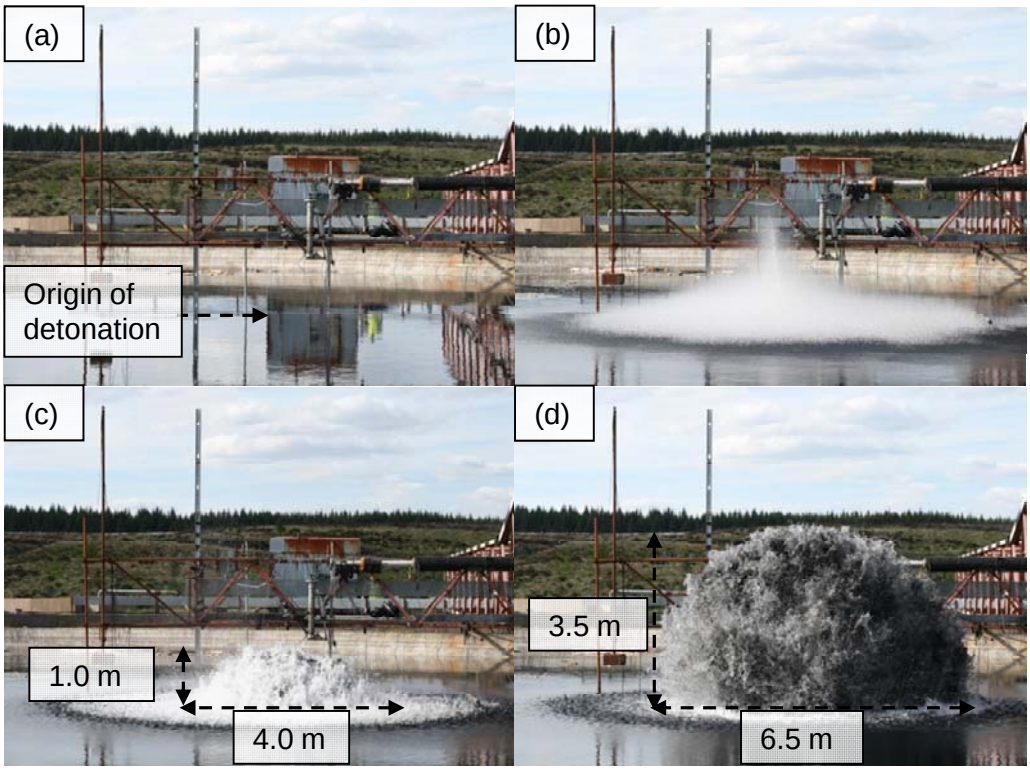

Figure 10: Images of the event taken from the edge of the pond of the water surface. Different stages of the blast event are shown: (a) Prior to detonation with various aspects of the set-up highlighted; (b) Initial shock wave reaching the surface of the water causing a spray of water to form at the surface; (c) Bubble migrating upwards forming a dome on the surface of the water (at ~ 1000 ms); (d) the bubble venting to the atmosphere throwing a mass of water into the air (at ~ 1400 ms).

Blast pressures experienced by panels G3 (30 mm core) and G4 (15 mm core) peaked at a shock pressure of 430 bar (1 kg of C4; 6 m depth; stand-off 1 m; panel air-backed) and 300 bar (1 kg of C4; 6 m depth; stand-off 1.4 m; panel water-backed) respectively. The two pressure-time traces are shown in Figure 11 for the two blast scenarios, illustrating the ferocity of the blast event, note that the strain gauge data will be restricted to the initial response also highlighted in Figure 11. Figure 12 shows an example of all strain gauge data for G4. These pressures are very high shock pressures to subject the test panels to and it resulted in significant damage sustained by the targets. The air-backed G3 had its core crushed to half the original thickness (*16 mm* core thickness reduction) by the shock. There were initial surface strains in the region of 3% and once the panel membrane response began, surface strains

of around 1% remained causing severe cracks to form within the skins along the panel edges. This is evident in Figure 13.

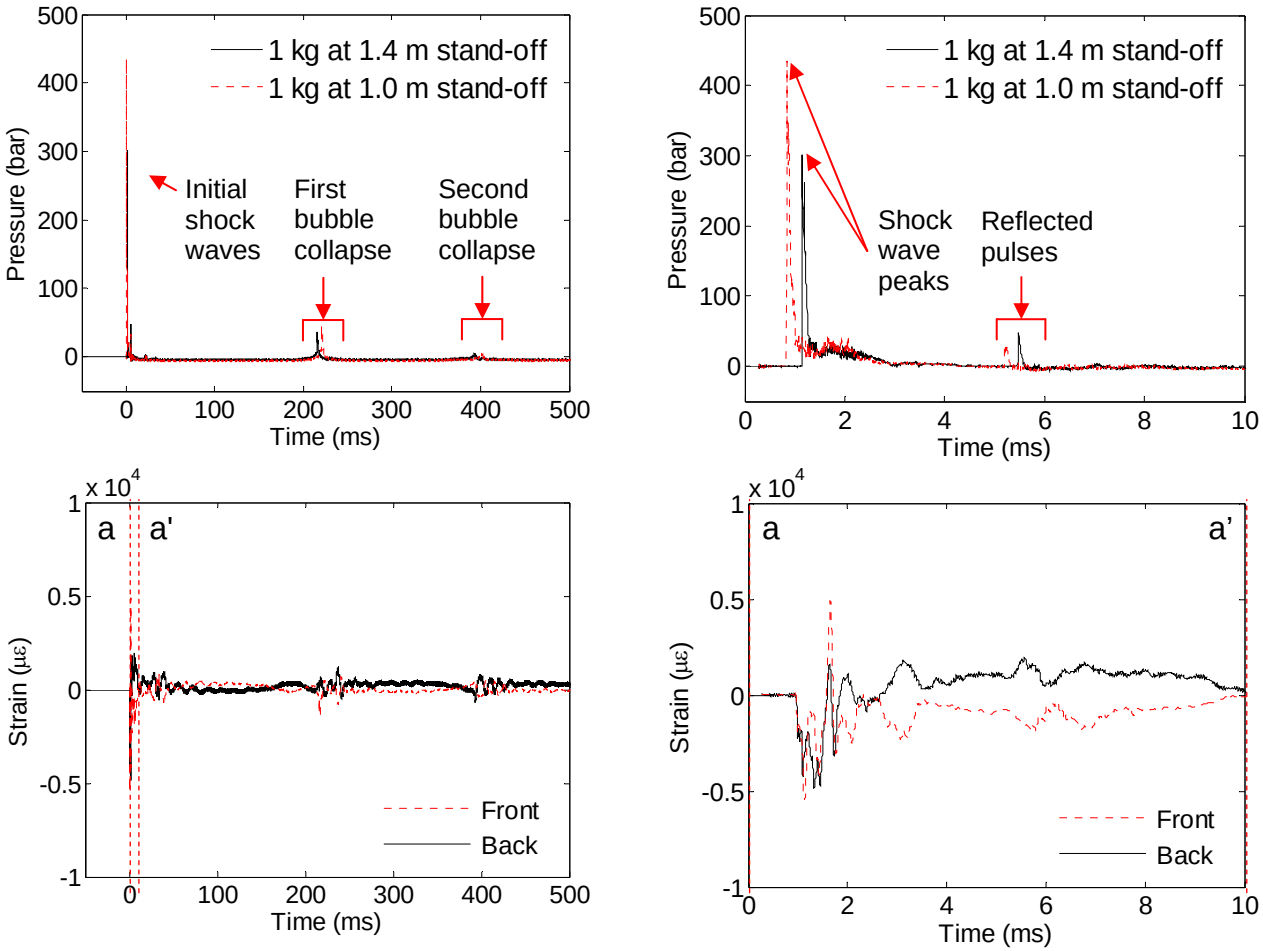

Figure 11: Pressure-time traces for 1 kg blasts at stand-offs of 1.0 and 1.4 m: the entire event including the 1st bubble pulse at ~ 200 ms (top left); and initial shock pressure including reflected shock at ~ 5 ms (top right). Sample strain gauge data of the panel response is given over these time periods for strain gauge position 1 (as shown in **Error! Reference source not found.**), front and back face, of the water backed-panel G4 (15 mm core thickness) when subjected to the 1 kg charge C4 at 1.4 m stand-off.

The water supporting the rear face of panel G4 was observed to dampen the overall response of the panel during the blast. The large strains observed in G3 were not observed in G4 due to the fact that the water medium supported the panel and restrained its response to the blast. Typical flexural response of the plate under a distributed transient pressure load was not observed. This is why surface strains generally remained low over the entire target area of G4 (water-backed) in comparison to the blast on G3 (air-backed), where strain magnitude rose towards the centre of the target. The fact that G4 experienced a decreased impulse was irrelevant; the change in the response characteristics is what has occurred. Figure 12 shows that strains peaked at ±0.6% on the front face and -0.6% on the back face of G4. Each face initially went into a state of compression, forcing the sandwich panel inwards on itself. After this, typical oscillatory motion ensued with strains of ±0.2% resulting. There was no visible

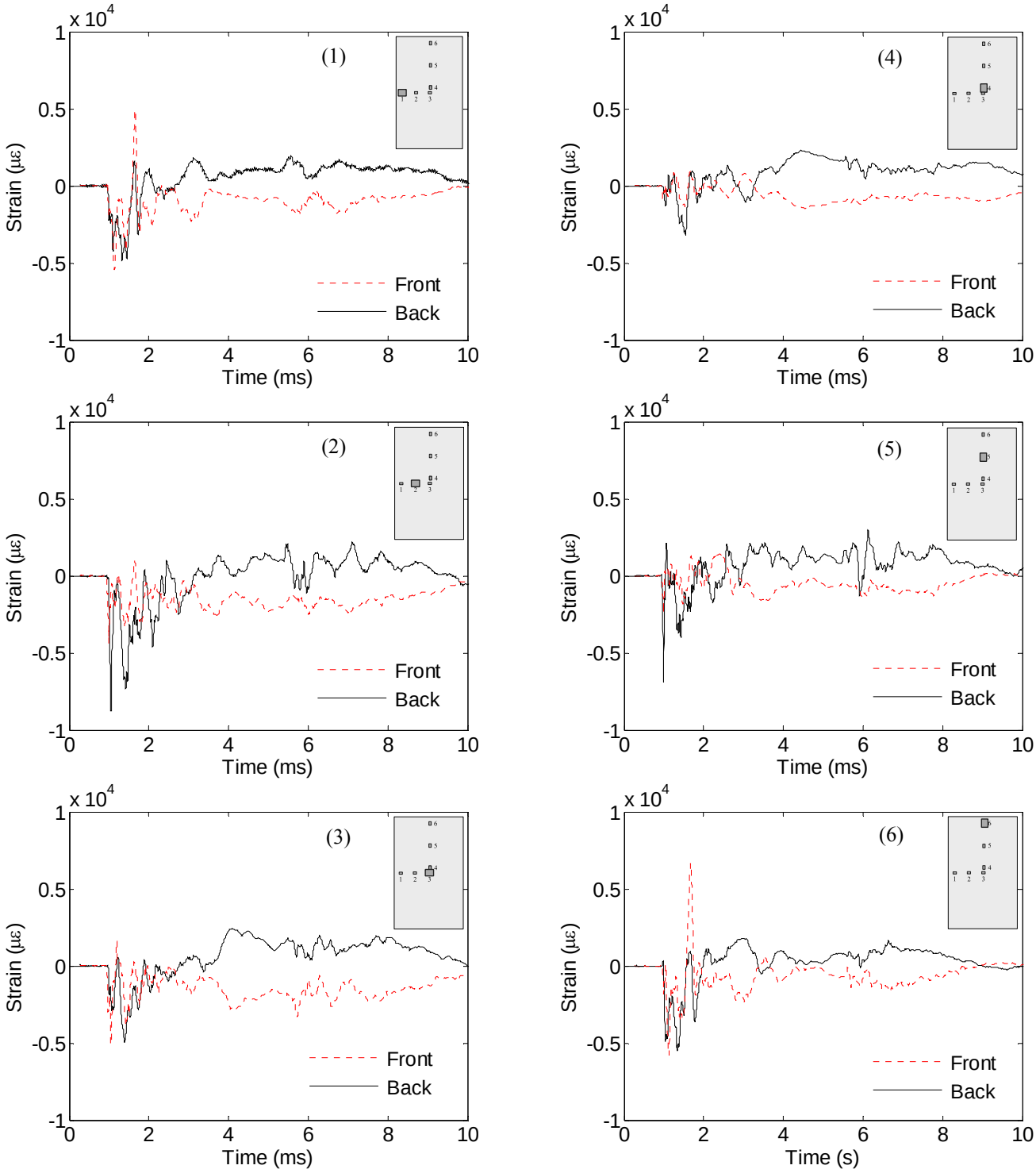

Figure 12: Sample strain gauge data displayed for G4 (core thickness 15 mm) sandwich composite panel with water on the front and back face (300 bar; 1 kg of C4; 6 m depth; stand-off 1.4 m). Data is displayed for the first 10 ms for each gauge position (numbered as shown in **Error! Reference source not found.**).

damage to the skins after the blast; however, the 15 mm thick core suffered significant crushing (7 mm core thickness reduction). This was again in the region of 50% core thickness reduction this time for a peak shock pressure of 300 bar (130 bar lower than that observed for G3) and an impulse of 4.82 bar ms (compared to 6.41 bar ms for G3). The two panel responses for G3 and G4 were compared in

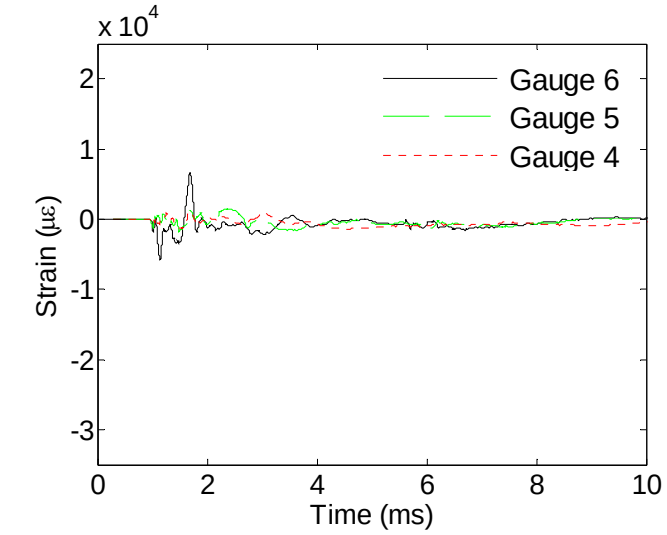

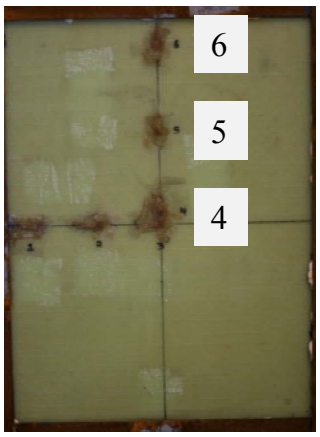

Front ~ no visible skin damage
Back ~ no visible skin damage
Core crushing ~ 7 mm

(a)

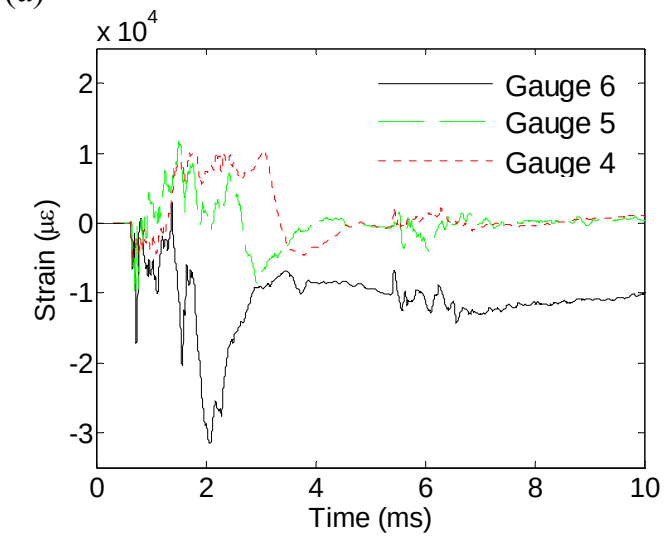

Front ~ skin creasing
Back ~ skin creasing/cracking
Core crushing ~ 16 mm

(b)

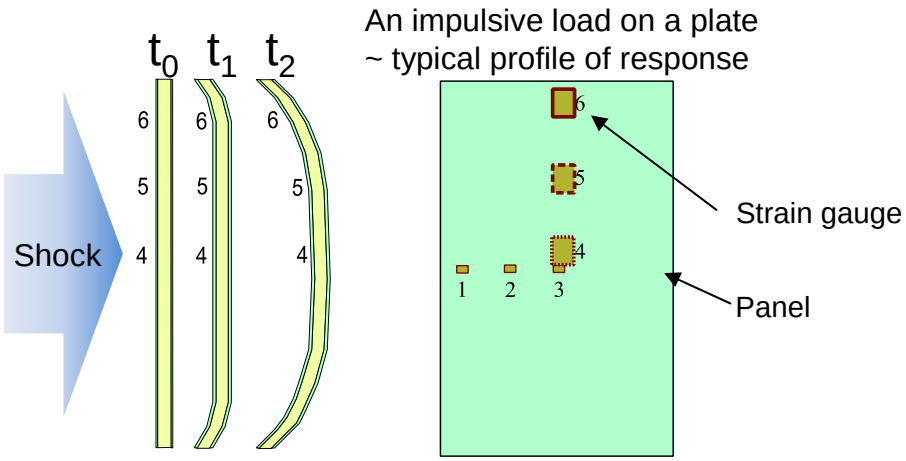

(c)

Figure 13: Comparison of underwater blast response of sandwich panels tested: The first 10 ms of strain gauge data is displayed for gauge positions 4-6 (numbered as shown in **Error! Reference source not found.**) for: (a) water-backed sandwich panel G4 (core thickness 15 mm) with shock: 300 bar (1 kg of C4; 6 m depth; stand-off 1.4 m); (b) air-backed sandwich panel G3 (core thickness 30 mm) with shock: 430 bar (1 kg of C4; 6 m depth; stand-off 1.0 m); (c) diagrammatic representation of G3 showing signs of typical impulsive behaviour with the top edge initially in compression whilst the remainder of the plate is in tension.

Figure 13, the difference in strain magnitude is highlighted as well as the effect of the backing medium with the water-backed G4 (see Figure 13(a)) experiencing lower surface strains compared to the air-backed G3 (see Figure 13(b)). Moreover the characteristic response of a plate due to impulsive loads was captured by the strain gauge data for the air-backed G3 illustrated in Figure 13(c). The plate experienced an initial compression near the top edge of the panel whilst the central region remained in tension as evident in the strain gauge response shown in Figure 13(b).

3.8 Underwater blast loading of GFRP tubular laminates

3.8.1 Progressive shock loading of GFRP tubular laminates

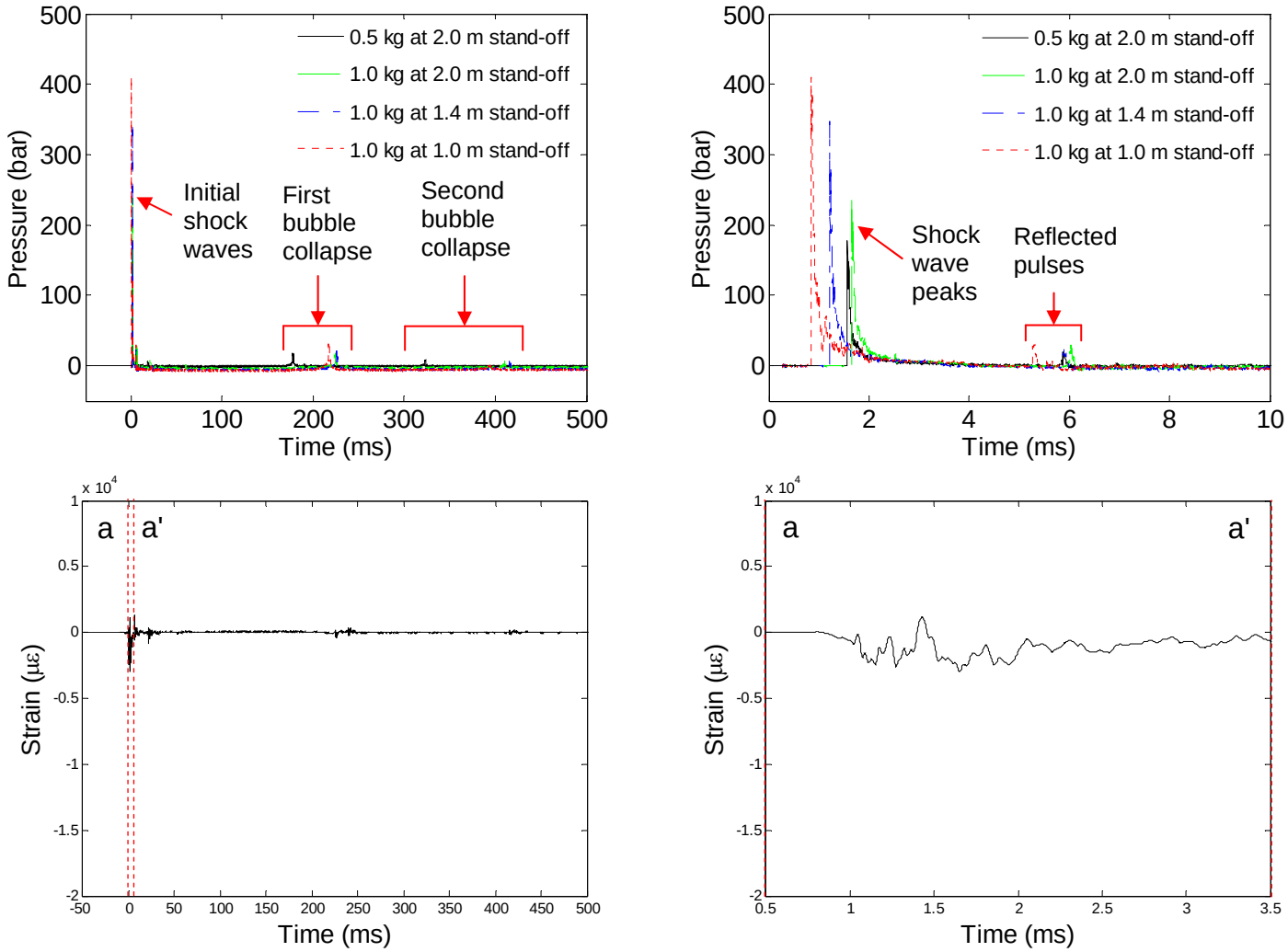

Figure 14: Pressure-time traces for 0.5-1.0 kg blasts at stand-offs of 1.0-2.0 m: the entire event including the 1st bubble pulse at ~ 200 ms (top left); and initial shock pressure including reflected shock from the water surface at ~ 5-6 ms (top right). Sample strain gauge data of the tubular laminate response is given over these time periods for strain gauge position 1 monitoring axial strain (as shown in **Error! Reference source not found.**) of the air-filled A1 when subjected to the 1 kg charge C4 at 1.4 m stand-off.

Figure 14 shows the combined pressure time traces for each underwater blast on composite tubular laminates of air-filled (AF) design. Peak pressures ranged from 180-400 bar for a range of blast parameters from 0.5 kg C4 explosive charge at a 2.0 m stand-off distance at a 6 m depth to a 1.0 kg charge at 1.0 m stand-off distance at the same depth. Figure 15 shows the combined results for the progressive loading of these tubular laminates. The 180 bar blast produced no visible skin damage to the targets with the surface strains sufficiently low to form an agreement with this observation. The 240 bar blast proved to be the threshold for damage evolution with surface strains reaching 1%. The tubes were then tested at a peak shock pressure of 350 bar and visible damage was inflicted on the targets with axial cracks forming along the front facing side of the sample as strains reached 1.5%. In the final test the tubes were taken beyond their limit, where complete shear failure was observed for a peak shock pressure of 400 bar. Similar signs of axial cracking were observed in this final sample (as for the blast of 350 bar) evident from the remains at the end-tabs featured in Figure 15 prior to the entire gauge length shearing off at the supports.

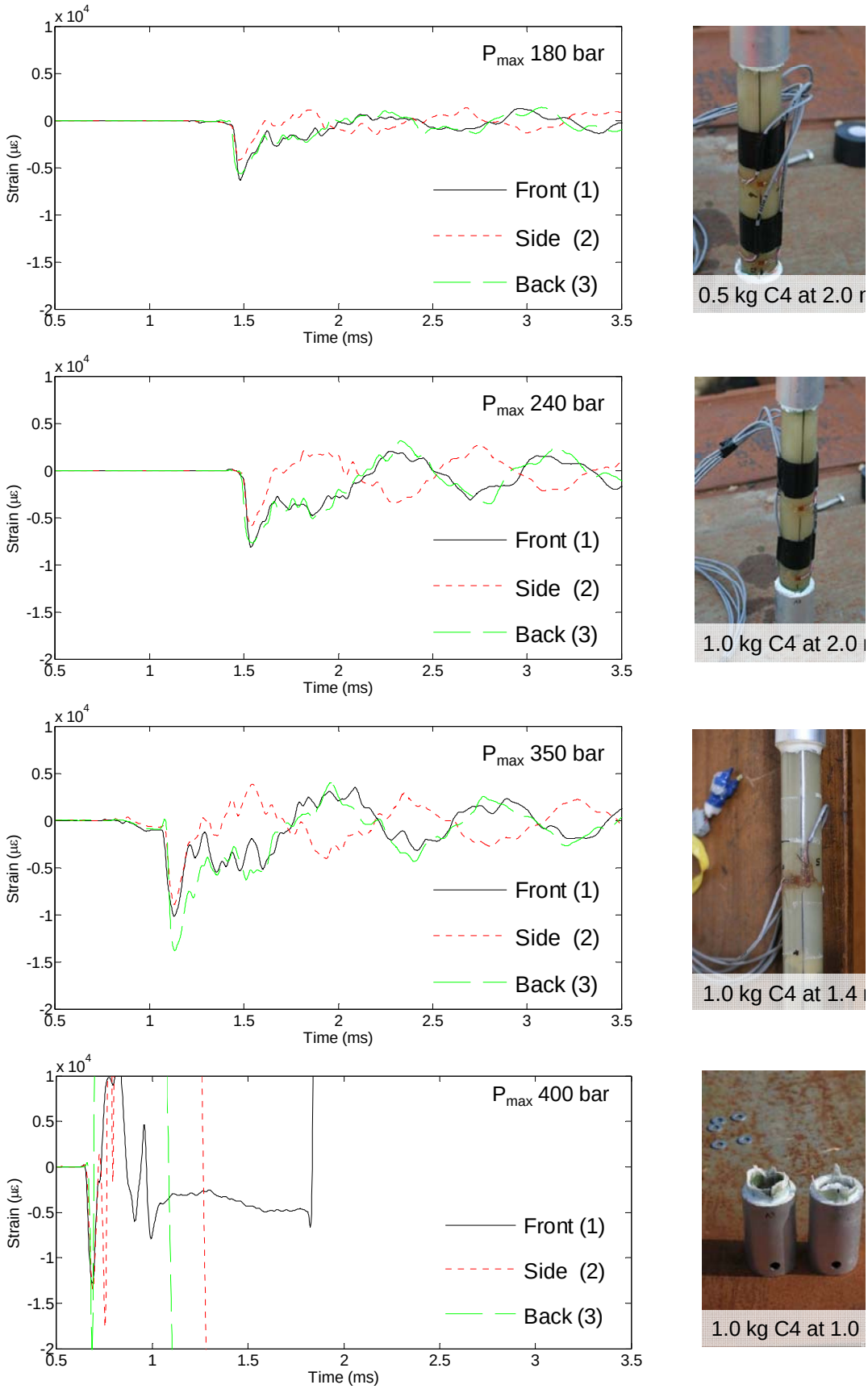

Figure 15: Shock loading of composite tubes with max shock pressure increasing from 180 to 400 bar.

3.8.2 Effect of filler fluid on tubular laminate response

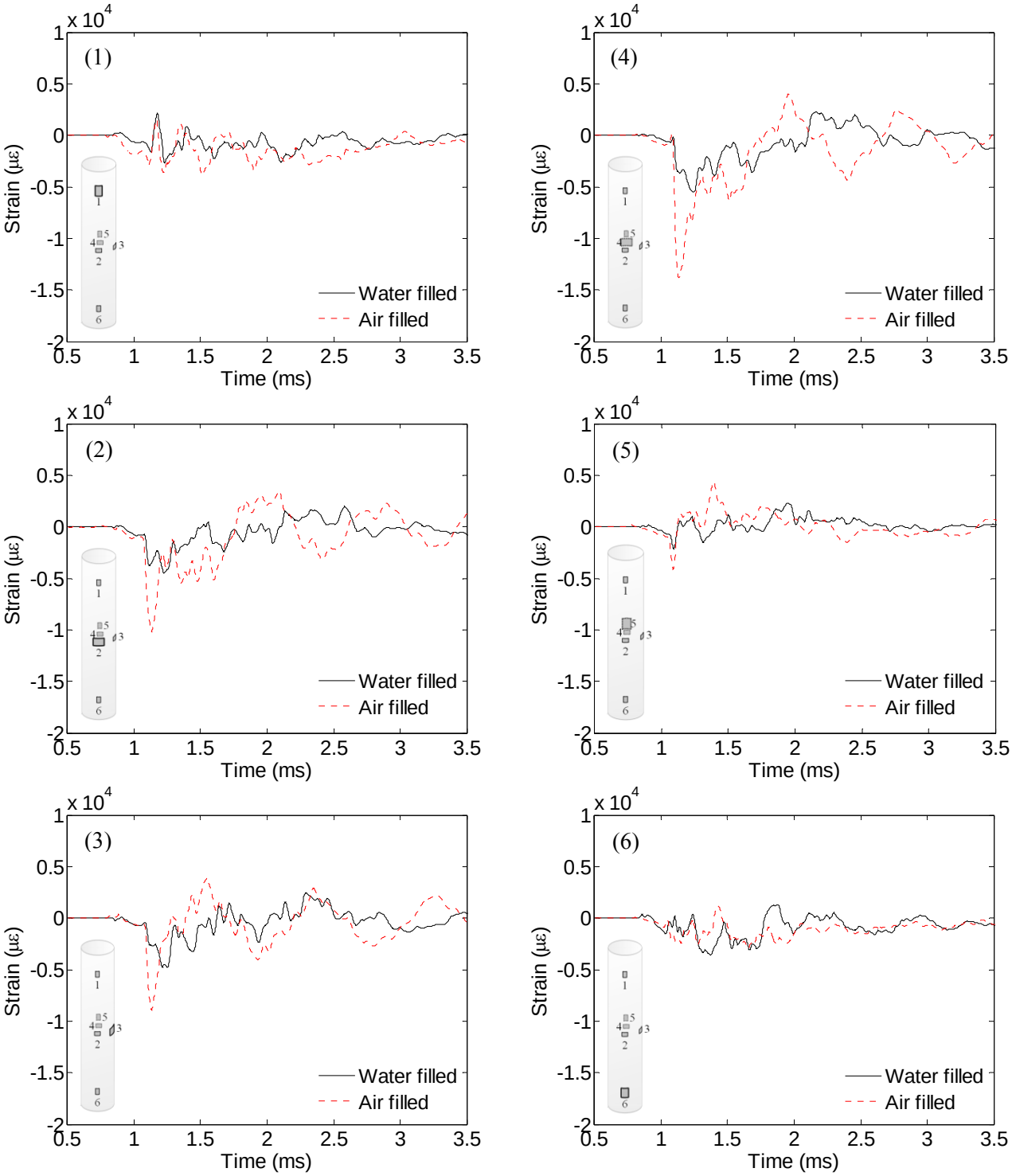

Figure 16: Strain gauge data is displayed for the first 3.5 ms with peak shock pressure of 350 bar (1 kg C4; depth 6 m; stand-off 1.4 m) for each gauge position on tubes AF and WF, each plot shows the corresponding data for AF (air filled) and WF (water filled) at that particular location.

One tube of each air filled (AF) and water filled (WF) design were subject to 350 bar peak shock load caused by a 1 kg C4 charge at 1.4 m stand-off at 6 m depth (pressure-time history shown previously in Figure 14). There is the initial compression/collapse of the tube inwards at its centre prior to the oscillatory squashing motion. However when these traces in gauges 2-4 for AF are compared to WF

(see Figure 16), there is a marked difference in response. Using water as the filler fluid causes a damped the amplitude of response, reducing peak strains from 1.5% in AF to 0.5% in WF (see gauge position 4 recording the fluctuation in hoop strain on the back facing side of the tube in Figure 16).

The tubes were both subject to a pressure of 350 bar (there were two independent recordings of pressure either side of the targets). The damage sustained by AF relative to WF was apparent with no visible damage observed for WF whereas AF shown in Figure 17 shows axial cracking, most likely caused by shear failure during the circumferential crushing phase of the sample deformation causing cracks to initiate.

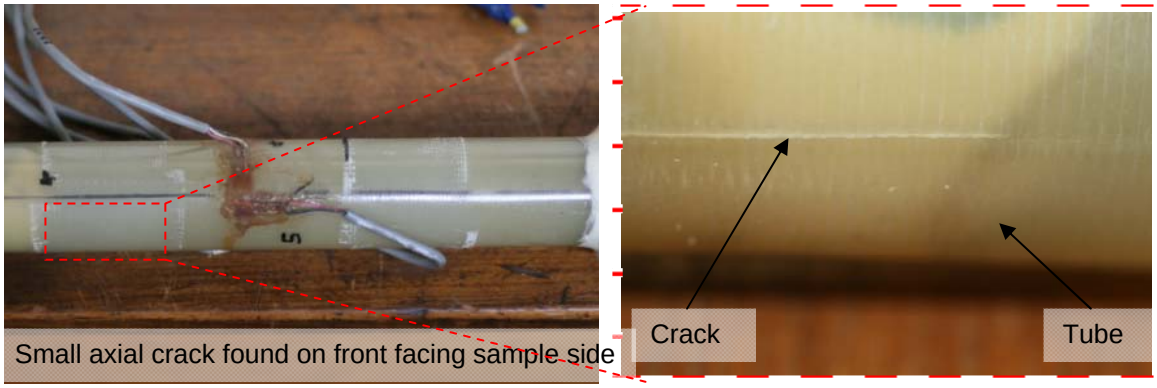

Figure 17: Post-test images of the AF tube (peak shock pressure of 350 bar) featuring axial cracking near one end (left) and a zoomed in view of the crack formed during the blast (right).

4 Discussion and analysis

These sandwich composite structures, although very simple in construction, provided significant blast resistance to shock loading. They sustained a pressure loading of 2 bar in air without resulting in a catastrophic failure. The back face of the panel still remained intact after deflecting 80 mm. The transition to underwater studies showed different energy absorbing and failure mechanisms. Core crushing and skin fibre breakage was observed but not complete skin-to-skin failure when subjected to peak shock pressures of 450 bar. The tubes represented an alternative geometry and the variable of filler medium proved to influence the response greatly.

4.1 Air blast loading of GFRP sandwich composite panels

A summary of the key results and observations from the air-blast loading of GFRP sandwich panels is given in Table 2. Comparing the response of G1 (40 mm core thickness) and G2 (30 mm core thickness) it was shown that the influence of increasing the core thickness lowered the amplitude of oscillations. Increasing the core thickness increases the second moment of area of the panel and the equivalent flexural rigidity, $(EI)_{eq}$. According to [19] $(EI)_{eq}$ is proportional to the square of the core thickness in sandwich materials. Therefore increasing the core thickness increased the stiffness of the panel and this provided for smaller peak amplitude of displacement. G1 was seen to deflect to a maximum distance out-of-plane of 63 mm whilst G2 deflected 78 mm. The first period of oscillation differed by only 10% between the two targets. Referring also to [16] discussing the response of a fully clamped panel to a uniformly distributed load, the equivalent single degree of freedom spring constant of the panel is proportional to $(EI)_{eq}$. Combining this stiffness term with the mass term, the natural

frequency can be determined. Therefore the period of oscillation was reduced for the thicker core, G1, given the stiffness term increased more significantly than the mass term, in this case by 10%, which was observed when referring to Figure 5 and Figure 6.

Table 2: Summary of each air-blast conducted on GFRP sandwich panels highlighting the peak pressures, peak strains and visible damage.

Sample code	Skin lay-up, core thickness (mm)	Charge size (kg), Stand-off distance (m)	Peak pressure (bar), duration (ms)	Peak strain (%)[1]	Damage	Notes
G1	2x QE1200, 40	30 kg; 14 m	2 bar; 6 ms	1	No visible damage	No damage detected in DIC analysis
G2	2x QE1200, 30	30 kg; 14 m	2 bar; 6 ms	1.25	No visible skin damage, some mild core cracks	Mild signs of damage visible in DIC
G1	2x QE1200, 40	30 kg; 8 m	8 bar; 5 ms	3	Severe skin and core cracking (no crushing)	Definite signs of damage shown in DIC as well as in post inspection

[1]Strain measurements were taken from the back face of the target.

The second G1 panel was tested with the 30 kg charge at 8 m, it can be seen when Figure 5 and Figure 8 are compared that G1 deflected over twice as much as during the blast at 14 m. The increased pressure (2 bar to 8 bar peak shock pressure) and impulse (0.43 bar ms to 1.25 bar ms) caused a more severe response from the target. There is a deviation from static analysis where, the response of a structure to an applied load will be expected to be proportional. These load cases discussed in this paper are highly rate dependent and the structural response is nonlinear. Furthermore introducing damage (and transient boundary conditions) can affect the energy absorbing mechanisms in action and therefore the amount of energy transferred to momentum in the plate.

In terms of damage when the second G1 panel was subject to a stronger blast a skin crack formed on the front face of the target. Employing DIC was a powerful tool for damage detection during the blast. The major principal strain fields generated can tell a great deal about what is happening to the structure. Referring to Figure 8 it is clear that there is a build up of high-strain of around 3% in the central region until a point, where there is a split in the strain field, with some strain relief appearing in a narrow region down the right-hand side of the panel. This region of stress relief indicates a region of separation between the core and skin (where the skin is unsupported by the core), resulting in the load concentrating on the edges of this (cracked-core) region on the skin. The levels of strain observed in the skin along these edges peaked at 1.8%. Further analysis in Figure 18 displays the deformed profile of the width of the panel. Out-of-plane displacement of a horizontal central section was taken within the ARAMIS post-processing software and plotted over regular time intervals for the duration of the initial response. It shows the panel deflecting in a symmetrical manner during its inward stroke, up until the point of maximum deflection occurring at 12.5 ms. It is clear that a failure (or change in structural balance) has occurred within the panel, causing an asymmetric rebound profile of the panel at 15.5 ms.

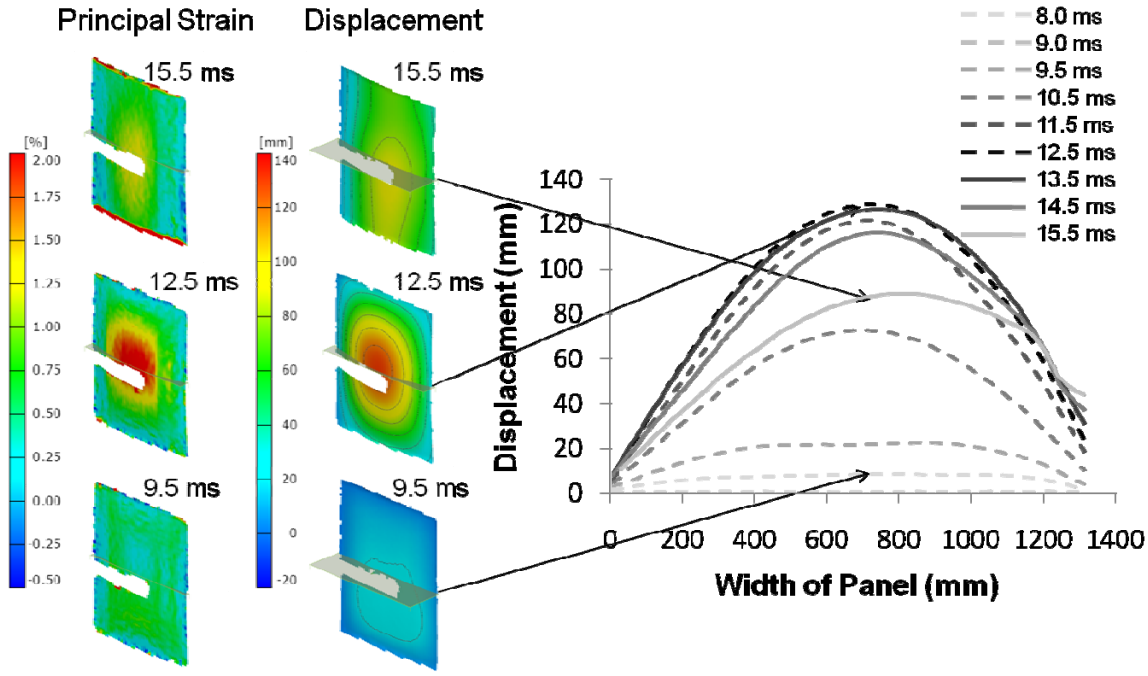

Figure 18: Displacement data taken across a horizontal section running through the point of maximum deflection for panel G1 (core thickness 40 mm) during blast loading (30 kg at 8 m stand-off). Data displayed for several time intervals from 8 ms after detonation. Dotted lines show displacement profile up to maximum deflection and solid lines show subsequent return.

This reinforces the notion of a complete core shear failure, resulting in complete crack propagation from face-to-face down a significant portion of the panel. The first 1.5 ms (8.0 to 9.5 ms) of response show the flat central area of the panel progressing, which is characteristic to impulsive loading situations. After 1.5 ms, there is a faint region of stress-relief on one edge of the panel due to crack initiation causing separation between the skin and core (locally). Now it can be accounted for due to the exaggerated bending stresses experienced in the early stages (around the square wave front) where the radius of curvature in the bend is significantly lower. The reason for the crack developing preferentially on one side rather than the other is due to the uneven loading experienced and the asymmetry in support conditions. The cubicle design is such that one edge of the composite sandwich panel leads to free air and one edge leads to the centre of the cubicle and so the magnitude of impulse deteriorates on one side relative to the other. This cubicle design also leads to an effectively more rigid support along the edge of the cubicle compared to the central support. For the ideal case (with the same support and loading all around the panel) cracks would be forming from all 4 corners causing a square section of the panel to crack. However, once one crack forms, stress relief dictates that another is unlikely to form without sustained or increased loading. Once the crack formed in the core the front (and back) skins were left unsupported by the core and therefore the strains concentrated on the edges of this core crack and this lead to skin fibre breakage. Sectioning confirmed that failures had occurred, specifically the core crack, which propagated through from face-to-face of the core (see Figure 9). However, the DIC analysis did pick up the separation of skin and core, also highlighted in the blast on G2 to an extent, confirmed with sectioning. With appropriate experience, DIC can be a very powerful tool for

monitoring the structural integrity of various materials and identifying damage mechanisms occurring even when subject to extreme load cases such as these.

4.1.1 Accuracy of data reported by DIC compared to laser gauge measurements

As stated previously, point data on the targets was taken from the DIC analysis and compared to the measurements recorded by a laser gauge for verification purposes (see Figure 19). Data was taken from the point where the laser gauge was targeting, which was precisely identified in the raw images. There was good agreement, with a <1% error until maximum deflection, between the two sets of measurements as shown in Figure 19(a). During the blast event, there reaches a point in time where the laser gauge (visibly) began to move and the data it was recording became compromised. The steel beam structure, comprising the mount for the laser gauge, flexed and vibrated after the (primary) target response reached peak deflection. To clarify when the laser gauge began to move, the steel beam itself was speckled and computed for its movements. It can be seen from Figure 19(b) that the position of the laser gauge begins to move at the point where the panel is reaching its maximum deflection. This data shows qualitatively where the reliability of the data deteriorates. After this stage the laser gauge begins to flex and rotate (observed in the video recording) and so the validity of its results breaks down, since it was not at its original start position nor was it pointing at the same point. This exercise indicated a close agreement of the two systems for point displacement measurements until the point of maximum deflection. Therefore the validity of the measurements taken using DIC techniques under such extreme conditions can be taken to be true (provided vibrations of the cameras can be kept to a minimum). Provisions of heavy based tripods, held down with auxiliary weighting, supporting the cameras isolated on rubber mounts ensured minimal vibration transmission until the target's 1st period of oscillation completed. To be conservative within this analysis, the DIC data is accepted until the 1st rebound. All data presented and discussed is taken from within this period.

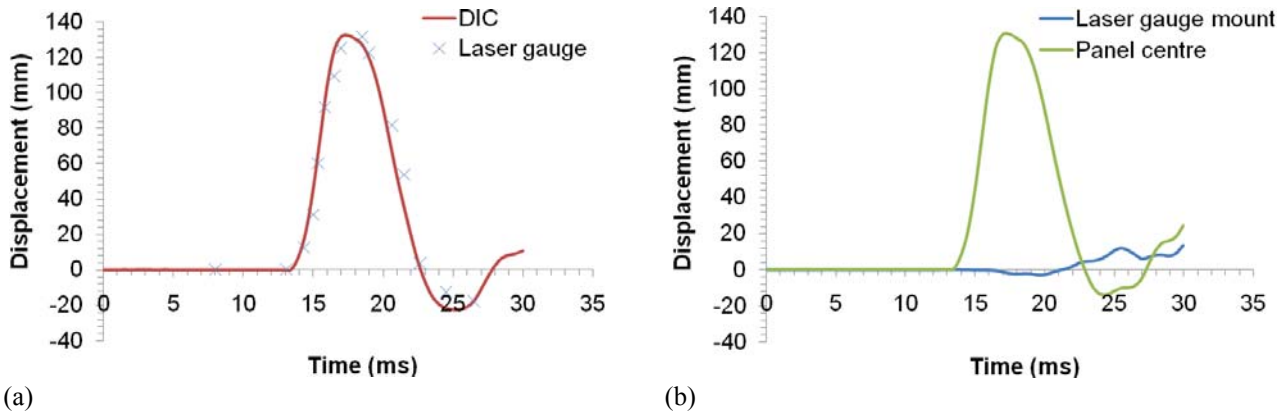

(a) (b)

Figure 19: Comparison of the central point displacement measured by the laser gauge and that recorded by the DIC analysis. The data shown is from the 30 kg at 8 m stand-off air-blast on G1: (a) analysis of the same point deflection during the blast measured by the DIC analysis and by the laser gauge; and (b) point data taken from the DIC analysis showing the relative movement of the laser gauge mount to its original target point on the panel.

4.2 Underwater blast loading of GFRP sandwich composite panels

Table 3: Summary of each underwater blast conducted on GFRP sandwich panels highlighting the peak pressures, peak strains and visible damage.

Sample code	Skin lay-up, core thickness (mm)	Charge size (kg), Stand-off distance (m)	Peak pressure (bar), duration (ms)	Peak strain (%)[1]	Damage	Notes
G4	2x QE1200, 15	1.0, 1.4 (water-backed panel)	300 bar 0.2 ms (peak) 3.0 ms (tail)	±0.6/-0.6	Severe core crushing but no visible skin damage	Water was present behind panel ~ squashing the panel during the blast
G3	2x QE1200, 30	1.0, 1.0 (air-backed panel)	430 bar 0.2 ms (peak) 3.2 ms (tail)	-3/-1[2]	Severe core crushing and skin cracking	Air was present behind panel ~ unsupported

[1]Strain measurements are shown for the front and back face of the target.
[2]Strain gauges lost the recording after the initial impact caused a given state of strain (compression).

As shown earlier with post-test images, significant damage was sustained by each target. Key observations and results are summarised in Table 3. The air-backed panel G3 (30 mm core thickness) had its core crushed to half the original thickness by the shock with pressure 430 bar (duration is stated in Table 3 as a duration of the peak, in this case 0.2 ms, and as a duration of the tail of the shock wave, which decays at a much slower rate than the initial stage, here the tail duration is 3.2 ms). By the time typical membrane response began, excessive surface strains remained in the region of 1% causing cracks to form within the skins along the panel edges. The front surface strain measurements for gauges 4-6 are displayed in Figure 13. From gauge 6 positioned at the top edge of the panel, it is clear that the panel bent, deformed around its edge, causing the 2-3% strains observed on the surface in that region. Comparing the strains across that length from edge to centre it is clear that after the initial compression, the centre moves into tension (unlike the panel edges), causing a possible 3rd order mode shape of flexural response. In other words the typical impulsive shape of deformation shown previously for the air-blast trials was present, where a square profile deforms outwards upon impact prior to parabolic oscillations. The resulting visible front-face damage concentrated around the top edge is shown previously in Figure 13. Although the initial shock can be assumed to act uniformly over the entire face, the bubble pulse would mainly have affected the top edge, given the 1st bubble minimum would have occurred 0.9 m above the site of the charge (calculations taken from [20]). This can account for the discrepancy of visible damage sustained by the top edge, since nearly half the explosive energy released by the charge contributes towards the pulsation of the bubble and this would have been imparted predominantly on the top edge of the panel.

For the water-backed shock loading of G4 thickness, by the shock with pressure 300 bar, it was shown that each face initially went into a state of compression, forcing the sandwich panel inwards on itself. This can be due to a number of reasons, namely, the panel being forced backwards against a mass of water and, due to the small time period and the fact that the water is encapsulated within the base-

frame, this caused an initial crushing effect (on the target) as there was insufficient means for the water to vent out of the frame (seals). This caused an increased through-thickness stress on the panel compared to when the panel is backed by air, resulting in the highly compressed core. The edges of the panel peaked into tension on both faces, perhaps as a response to the compression of the core or superposition of surface stress waves at the boundary edge. After this, typical oscillatory motion ensued with strains of ±0.2% resulting. There was no visible damage to the skins after the blast due to the relatively low surface strains experienced. The 15 mm thick core however was crushed to nearly half its original thickness due to this pressurising effect. The difference between the two underwater blasts in terms of peak shock pressure and the backing medium meant that for the lower peak shock pressure the same relative core thickness reduction was experienced, simply due to the fact that the backing medium was denser. This phenomenon was verified in another set of trials where two targets of same thickness were subject to the same peak shock pressure with only the backing medium the variable. The air backed panel sustained more skin damage but less core crushing due to the nature of the fluid medium supporting the skins.

4.3 Underwater blast loading of GFRP tubular laminates

The results are summarised in Table 4 for both the progressive loading of GFRP tubular laminates as well as the experiments to observe the effect of the filler medium.

Table 4: Summary of each underwater blast on GFRP tubular laminates highlighting the peak pressures, peak strains and visible damage.

Sample code	Charge size (kg), Stand-off distance (m)	Peak pressure (bar), duration (ms)	Peak strain (%)[1]	Damage	Notes
AF	0.5, 2.0	180 bar 0.1 ms (peak) 2.4 ms (tail)	-0.2/0.3/±0.2	No visible damage	Elastic oscillations
AF	0.5, 2.0	180 bar 0.1 ms (peak) 2.4 ms (tail)	-0.6/-0.6/-0.4	No visible damage	Elastic oscillations
AF	1.0, 2.0	240 bar 0.1 ms (peak) 2.3 ms (tail)	-0.4/0.4/±0.3	Some surface fibre damage visible	Elastic oscillations but subsurface damage to laminate
AF	1.0, 2.0	240 bar 0.1 ms (peak) 2.3 ms (tail)	-0.7/-0.8/-0.5	Some surface fibre damage visible	Breathing motion clearly observed with larger amplitude strains
AF	1.0, 1.0	400 bar 0.2 ms (peak) 3.0 ms (tail)	±1/+ve/+ve[2]	Complete shear failure at the ends of the tube	The central section began to respond prior to fracture at ends
AF	1.0, 1.0	400 bar 0.2 ms (peak) 3.0 ms (tail)	±1/ 3/ ±1[2]	Complete shear failure at the ends of the tube	The central section began to respond prior to fracture at ends
AF	1.0, 1.4	350 bar 0.1 ms (peak) 2.3 ms (tail)	-1/-1.5 -1	Axial cracking at front face ends of tubes	Hoop strains dominated with larger amplitude of strains
WF	1.0, 1.4	350 bar 0.1 ms (peak) 2.3 ms (tail)	±0.3/-0.5 -0.4	No visible damage	Filler fluid damped the strains experienced

[1]Strain measurements are shown for the front, back and side of each tube.
[2]Strain gauges lost the recording after the initial impact caused a given state of strain (tension).

4.3.1 Progressive shock loading of GFRP tubular laminates

This set of blasts produced progressive damage on the tube constructions from no visible damage to complete shear failure, when subjected to peak shock pressures of 180 bar to 400 bar. For the blast of 0.5 kg at 2 m producing a peak shock pressure of 180 bar, 0.1 ms duration, the gauge data indicated mild bending response with opposing axial strain gauges recorded signals that were out-of-phase with each other i.e. one in tension when the other is in compression; and initial breathing action hoop strains were all in compression (-0.6%). After this (0.5 ms after impact) the tube response reverts to an oscillatory squashing motion (front/back strain gauges were out-of-phase with side strain gauges), see Figure 15 for hoop strain data.

This air filled (AF) construction was tested to a peak shock pressure of 240 bar, 0.1 ms duration, (1.0 kg at 2 m stand-off). This blast resulted in larger amplitude of strains of similar characteristics to the

previous blast (0.5 kg at 2 m). Strains peaked at 0.8% across the range of gauges. There were generally only mild signs of possible damage with chalky patches appearing on the tube surfaces (mild matrix cracking). This was the threshold for damage for this construction. The AF tube was then subject to a peak pressure loading of 350 bar, 0.1 ms duration, (1.0 kg at 1.4 m stand-off), which resulted in axial cracks forming at the front ends of the tubes. The characteristic response of the tube was again similar to that those tested previously with strain peaking at 1.5%, highlighted in Figure 15. The final blast, 1 kg at 1 m stand-off, on AF tubes exceeded the blast limit of the tube construction when subject to a peak pressure of 400 bar, 0.2 ms duration. From the strain data in Figure 15 it is clear that the tubes response was insufficient to absorb the energy imparted on it in a quick enough period. The strain gauge recordings implied an initial compression inwards, with the front face circumferential gauge holding at 0.5% strain, prior to the ends of the tube shearing away from the fixed end-tabs, terminating all recordings within the first 5ms.

4.3.2 Effect of filler fluid on tubular laminate response

All common modes of response expected by tube structures to underwater shocks were present as mentioned in the previous section of analysis: circumferential reduction/expansions (breathing) and elliptical oscillations (squashing) as illustrated in Figure 20. The tubes represent an alternative geometry to the flat panels. The initial shock wave wraps around the cylindrical geometry, causing an inward compression. After the pressure of the surrounding fluid reduces the energy gone into deforming the tube in this manner is released in the mode of oscillatory vibrations with the dominant mode in the form of a circumferential squashing motion. These two modes of vibration were the most dominant of those observed during these trials, however, the most significant result to emerge from this trial is the fact that the backing fluid (filler fluid) made considerable savings with regard to damage sustained by the tube structures (visible in Figure 17). The denser filler medium (water) made the tube effectively more rigid and reduced the magnitude of surface strains experienced and hence damage sustained. Figure 16 shows that the water filled tube experienced surface strains of half the magnitude of those experienced by the air-filled tube. To analyse this further, having a denser filler medium also dampens the vibrations quicker. After a few milliseconds, the strains in the air-filled tube are still greater than even the maximum strain experienced by the water filled tube. Moreover the water-filled tube seems to also resist the elliptical/squashing mode of vibration clearly observed with the air-filled tube. This is due to the fact that the tube needs to compress the filler medium to oscillate between tension/compression when going through this squashing motion and the energy required to compress the denser filler medium is too great. Therefore the energy is dissipated within the water filler medium and in mild residual surface vibrations in comparison to the air-filled tube which freely vibrates with large magnitude of strains >1% (highlighted in Figure 20).

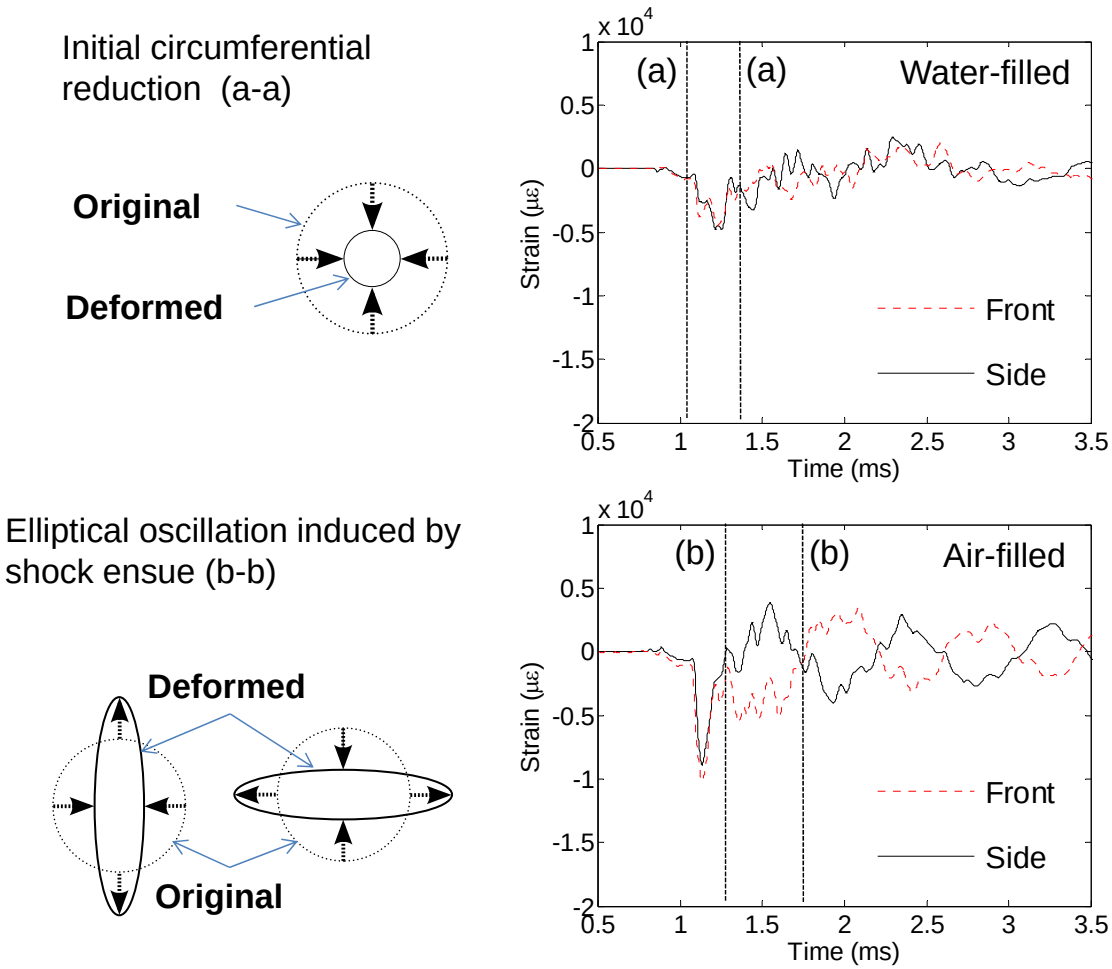

Figure 20: Diagram illustrating the 2 main modes of deformation observed, breathing (top left) and elliptical oscillation or squashing (bottom left) as the relative magnitudes of strain observed in both tube cases, water filled (top right) and air-filled (bottom right).

5 Conclusions

These sets of blast data have shown the capabilities of simple constructions to resist blast loads. Both conventional (strain gauges) and more advanced (high-speed DIC) strain monitoring techniques were employed to monitor the deformation of the targets during the blasts. Various aspects of blast events have been highlighted by these studies such as the ferocity of the blasts, the damage they can inflict as well as how boundary conditions can affect the outcome in terms of damage sustained and how these boundary conditions can play more of an important role in blast mitigation than material design. During the underwater trials the sandwich panels were subject to pressures over 10 times greater in magnitude in less than a tenth of the period of time than those experienced during the air-blast trials. During the air-blast trials back-face skins (and front-face skins generally) maintained their form without tearing/cracking. However during the underwater blasts, the cores experienced considerable crushing (up to 50%) and the skins experienced very large strains, causing fibre breakage on both faces (with strains exceeding 3%) when the targets were backed by air. The effect of having water as a backing medium reduced the surface strains experienced and hence damage incurred by the skins but increased the relative crushing observed in the core. Tube structures were tested and the effect of the filler/backing medium was again apparent with the water filled tube reducing surface stains by 60% in

some regions. The sample data is limited for traditional statistical analysis of sample response (no repeat experimentation). This is due to the fact that the samples used were full-scale and restrictions were in place with respect to the consumables required to manufacture them. However, within the small sample of tests conducted, verification of the data collected for the air-blasts was achieved to some extent using two techniques for point measurement and for the underwater-blasts using multiple gauge arrangements, giving confidence in the quality of data recorded.

The main findings in summary are:

- DIC was successfully employed during full-scale air-blast experiments to capture the damage progression in sandwich GFRP structures.
- There is a difference in response of GFRP sandwich panels to air-blast (30 kg at 8-14 m) and underwater-blast loading (1.0 kg at 1.0-1.4 m) due to the different pressure-time signatures: peak shock pressures of 2-8 bar (6 ms duration) to 300-430 bar (0.2 ms duration).
- Damage mechanisms changed from front-face skin damage and core shear cracking for air blast to severe core crushing (up to 50 %) and skin fibre-breakage for underwater blast.
- Damage and response of tubes subjected to underwater blast varies according to whether the tubes are filled with air or water, with the air-filled tubes sustaining longitudinal cracking compared to no visible damage on the water-filled tube subject to the same blast load.
- All experiments, on blast loading of GFRP structures, highlighted the importance of boundary conditions on the structural response and damage sustained by the structure, in terms of both location and nature of damage caused by a blast.

6 Acknowledgements

Much appreciated is the strong support received from Dr Yapa Rajapakse of the Office of Naval Research (ONR N00014-08-1-1151) in particular for Hari Arora. We also acknowledge the Metropolitan Police and CPNI for use of the test cubicles and other equipment, GL Industrial for the use of their facilities and support on site, SP Gurit for provision of materials and GOM mbH for access to latest DIC equipment during the air-blast trials.

7 References

1. Neuberger, A., Peles, S. and Rittel, D., *Scaling the response of circular plates subjected to large and close-range spherical explosions. Part I: Air-blast loading.* International Journal of Impact Engineering, 2007. 34(5): p. 859-873.
2. Neuberger, A., Peles, S. and Rittel, D., *Scaling the response of circular plates subjected to large and close-range spherical explosions. Part II: Buried charges.* International Journal of Impact Engineering, 2007. 34(5): p. 874-882.
3. Tekalur, S.A., Shukla, A. and Shivakumar, K., *Blast resistance of polyurea based layered composite materials.* Composite Structures, 2008. 84(3): p. 271-281.
4. Tekalur, S.A., Shivakumar, K. and Shukla, A., *Mechanical behavior and damage evolution in E-glass vinyl ester and carbon composites subjected to static and blast loads.* Composites Part B-Engineering, 2008. 39(1): p. 57-65.
5. Tekalur, S.A., Bogdanovich, A. E. and Shukla, A., *Shock loading response of sandwich panels with 3-D woven E-glass composite skins and stitched foam core.* Composites Science and Technology, 2009. 69(6): p. 736-753.

6. Hoo Fatt, M.S., and Palla, L., *Analytical Modeling of Composite Sandwich Panels under Blast Loads.* Journal of Sandwich Structures & Materials, 2009. 11(4): p. 357-380.
7. Wang, E.H. and Shukla, A., *Analytical and experimental evaluation of energies during shock wave loading.* International Journal of Impact Engineering, 2010. 37(12): p. 1188-1196.
8. Jackson, M. and Shukla, A., *Performance of sandwich composites subjected to sequential impact and air blast loading.* Composites Part B: Engineering. In Press, Corrected Proof.
9. Cole, R.H., *Underwater Explosions,* 1948: Princeton Univ. Press.
10. Hetherington, J.G., and Smith, P.D., *Blast and Ballistic Loading of Structures*1994: Butterworth Heinmann.
11. Panciroli, R. and Abrate, S., *Dynamic Response of Sandwich Shells to Underwater Blasts*. in *ICCM 17*. 2009. Edinburgh, UK: IOM Communications.
12. Deshpande, V.S., Heaver, A. and Fleck, N.A., *An underwater shock simulator.* Proceedings of the Royal Society A-Mathematical Physical and Engineering Sciences, 2006. 462(2067): p. 1021-1041.
13. Espinosa, H.D., *Performance of composite panels subjected to underwater impulsive loading*. in *ONR 2009 Solid Mechanics Program*. 2009. UMUC, Maryland.
14. LeBlanc, J. and Shukla, A., *Dynamic response and damage evolution in composite materials subjected to underwater explosive loading: An experimental and computational study.* Composite Structures, 2010. 93(3): p. 1060-1071.
15. Rajendran, R., Paik, J.K. and Lee, J.M., *Of underwater explosion experiments on plane plates.* Experimental Techniques, 2007. 31(1): p. 18-24.
16. Biggs, J.M., *Introduction to Structural Dynamics,* 1964: McGraw-Hill Book Company.
17. Deegan, M., *Email - Strain gauge application to underwater explosive events*, 2010.
18. Kwon, Y.W. and Fox, P.K., *Underwater Shock Response of a Cylinder Subjected to a Side-on Explosion.* Computers & Structures, 1993. 48(4): p. 637-646.
19. Gibson, L.J. and Ashby, M.F., *Cellular solids, structure and properties*. Second ed. Cambridge Solid State Science, 1997: Cambridge University Press.
20. Reid, W.D., *The response of surface ships to underwater explosions*, 1996, Department of Defence, Defence Science and Technology Organisation.